CHALMERS
UNIVERSITY OF TECHNOLOGY

LICENTIATE THESIS

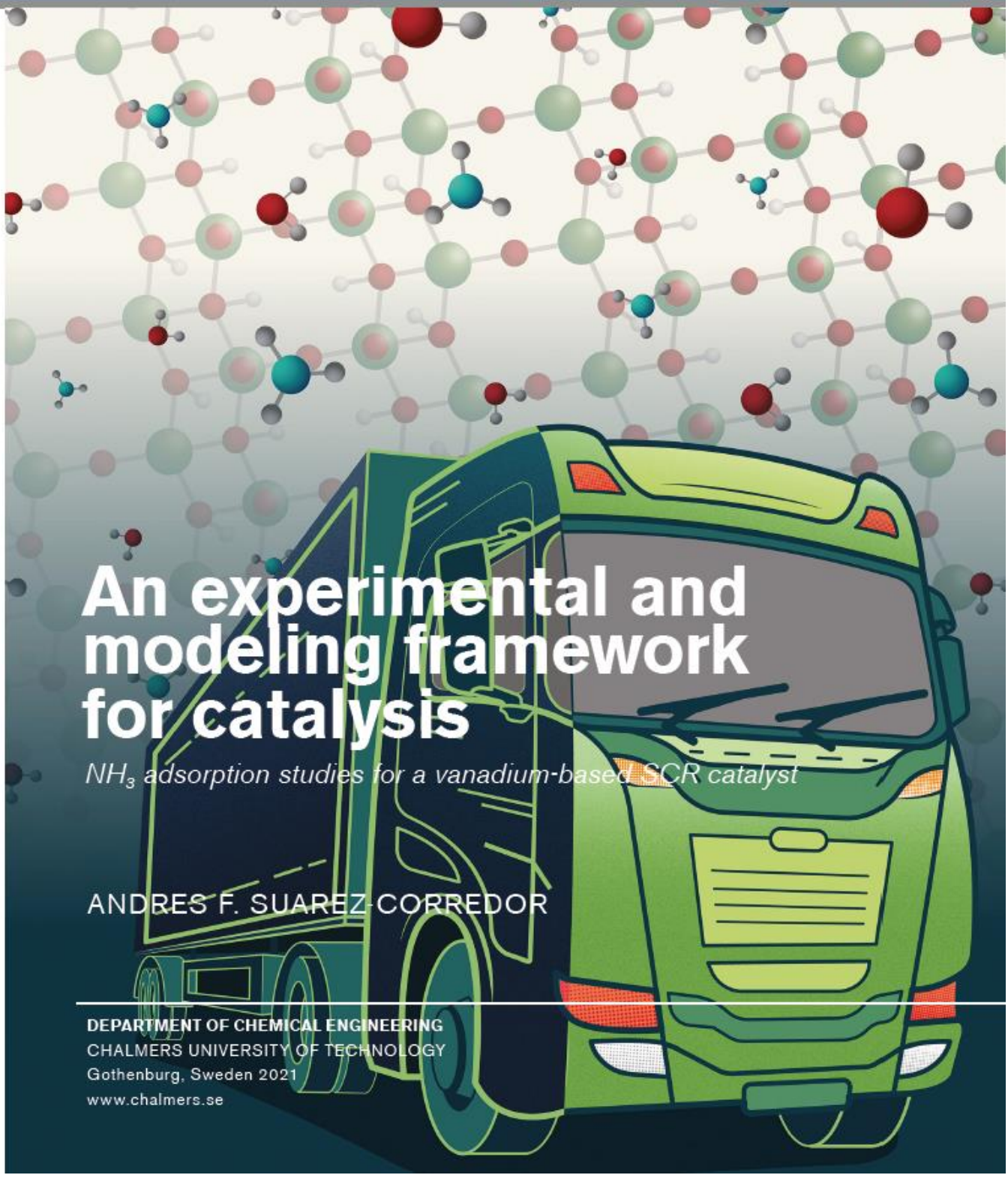

An experimental and modeling framework for catalysis

NH_3 adsorption studies for a vanadium-based SCR catalyst

ANDRES F. SUAREZ-CORREDOR

DEPARTMENT OF CHEMICAL ENGINEERING
CHALMERS UNIVERSITY OF TECHNOLOGY
Gothenburg, Sweden 2021
www.chalmers.se

ANDRES F. SUAREZ-CORREDOR
An experimental and modeling framework for catalysis
2021

THESIS FOR THE DEGREE OF LICENTIATE OF ENGINEERING

An experimental and modeling framework for catalysis

Andres F. Suarez-Corredor

Department of Chemical Engineering
Chalmers University of Technology
Gothenburg, Sweden, 2021

An experimental and modeling framework for catalysis

Andres F. Suarez-Corredor

Licentiatuppsatser vid Institutionen för kemi och kemiteknik
Chalmers tekniska högskola
Nr 2021:21
This thesis has been prepared using LaTeX.

Department of Chemical Engineering
Chalmers University of Technology
SE-412 96 Gothenburg, Sweden
Phone: +46 (0)31 772 1000
www.chalmers.se

Printed by Chalmers Reproservice
Gothenburg, Sweden, August 2021

Abstract

Internal combustion engines will have an important role towards sustainable transportation at least in the medium term. New emission legislation is aiming to a further decrease on pollutants and an increase of fuel efficiency. The latter could increase NO_x emissions which will require more understanding of the features and reaction mechanisms for Selective catalytic reduction (SCR) catalysts used in the emission after-treatment system for NO_x reduction.

In a vanadium-based SCR catalyst, NH_3 adsorption is one of the main steps in the SCR reaction mechanism affecting catalyst performance under transient conditions depending on temperature, gas concentration and vanadium oxidation state. Thus, modelling of NH_3 adsorption for industrial application is a challenge as it demands precision, accuracy and robustness required by the new legislation. Therefore, new experimental methods and modeling strategies are needed to capture valuable information and maximize data utilisation from experiments.

In this thesis, a new experimental and data pre-processing method was developed using a gas flow reactor for obtaining NH_3 adsorption isotherms over a wide experimental region suitable for modeling purposes. Then, an NH_3 adsorption model is proposed by a data-drive modeling process. First, a large set of candidate models was generated based on an array of feasible adsorption mechanisms. Then, parameter estimation was performed using different objective functions with increased complexity improving convergence. Finally, a robust model was achieved by a cross-validation and quality assessment step.

As a result, the best selected model for NH_3 adsorption over a vanadium-based SCR catalyst involves five adsorption sites: one site with a simple NH_3 adsorption mechanism, three sites with a competitive adsorption mechanism and one site with a water activated adsorption mechanism. The model can describe two phenomena impacting NH_3 storage: surface water dynamics, adsorption or dissociation, and vanadium oxidation states. Moreover, model parameters show physical significance related to studies at molecular level. The proposed experimental and modeling method will prove useful in developing complex kinetic models with increased validity and extended application.

Keywords: Vanadium-SCR, kinetic modeling, parameter estimation, NH_3 adsorption.

List of Publications

This thesis is based on the following publications:

[A] **A. Suarez-Corredor**, M. Bäbler, L. Olsson, M. Skoglundh, and B. Westerberg, "Characterization method for Gas flow reactor experiments - NH_3 Adsorption on vanadium-based SCR catalysts". Published in Ind. Eng. Chem. Res., 2021, 60, 30.

[B] **A. Suarez-Corredor**, M. Bäbler, L. Olsson, M. Skoglundh, and B. Westerberg, "A multi-scale modeling approach to the nature of active sites for a vanadium-based SCR catalyst: NH_3 adsorption studies". Manuscript.

Acknowledgments

The research in this thesis is sponsored by Scania CV AB within the Competence Centre for Catalysis (KCK) at Chalmers University of Technology, Göteborg, Sweden. The Competence Centre for Catalysis is financially supported by the Swedish Energy Agency and the member companies AB Volvo, ECAPS AB, Johnson Matthey AB, Preem AB, Scania CV AB, Umicore Denmark Aps., and Volvo Car Corporation AB. Furthermore, I acknowledge Umicore for providing the catalyst samples used in this research.

Additionally, I would like to thank:

My main supervisor, Björn Westerberg, for being a mentor in this project and my personal development. I am fortunate to work with a person willing to share his knowledge and experience, always being available for discussing and finding solutions. Your unconditional support and kindness made me appreciate and enjoy this project as its fullest.

My co-supervisor, Matthäus Bäbler, for taking the decision to participate in this project, his invaluable feedback, and never ending support and ideas thriving always to excellence. Your energy for giving the best is contagious.

My other co-supervisors and collaborators at Chalmers, Louise Olsson and Magnus Skoglundh, for their advises, feedback and enthusiasm in having fruitfully discussions.

I also want to thanks my colleagues at Scania, in the NXPK group, specially to Charlotta, Petra, Sara and Pak. Your energy, technical discussions and coffee chats make this project more enjoyable. I am very lucky to share my work life with you. Furthermore, I want to thank Karl Rejnö and Klas Oloffson for giving me the opportunity to work at this company and trusting on my skills for this job.

My wife and best friend, Margarita, for giving me happiness in my life, and helping me with your understanding and patience on reaching my best results in this project. I am immensely grateful that you decided to be part of our adventure in Sweden. Finally, my family, for their unconditional support, for teaching me to live and become the person I want to be: a happy one.

Acronyms

SCR:	Selective catalytic reduction
AIC:	Akaike information criterion
DFT:	Density functional theory
RTD:	Residence time distribution
EPA:	U.S. Environmental protection agency
MFC:	Mass flow controller
FTIR:	Fourier-transform infrared spectroscopy
GHG:	Greenhouse gases
TPD:	Temperature Programmed desorption
LSS:	Least square sum

Contents

Part I

Overview

CHAPTER 1

Preface

1.1 A sustainability standing

Sustainable development is defined as development that "meets the needs of the present without compromising the ability of future generations to meet their own" [1]. Therefore, sustainable transportation involves the implementation of this concept using technology, policies, and new social and economical constructs. However, a single path towards sustainable transportation is impossible since the utilisation of technology and science depends on the values, moral, and ethical standing we have as a society.

The utilisation of technology and a sustainability road-map is case specific, but the responsibility as researchers lies on the supply of facts, solutions and tools for the society to develop and also to make informed decisions. The transportation sector as a result of its diversity and relevance, is full of solutions and sustainability road-maps which can be contradictory sometimes. However, all of these solutions and road-maps have in common an anthropocentric view on the environment, since they see the Earth and its resources as a service provider for our fulfilment. Some services we get from the ecosystem are illustrated in Fig. 1.1.

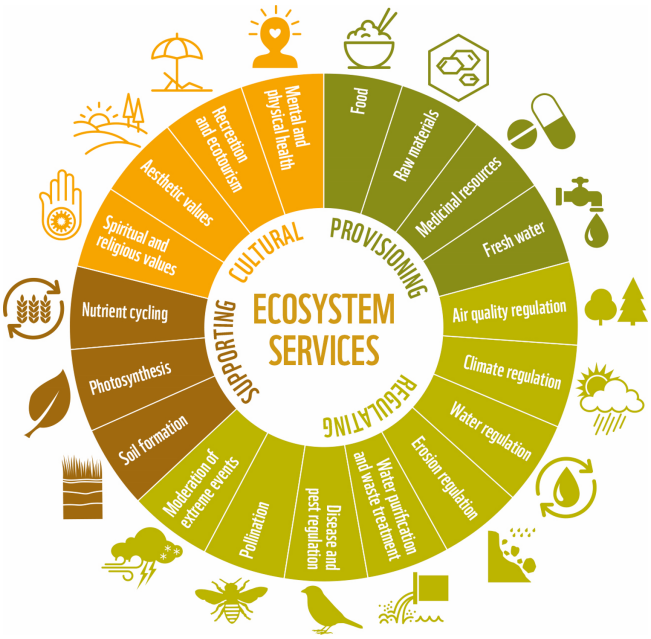

Figure 1.1: Ecosystem services. Taken from [2]

.

Legislation on transportation has mostly been focused on emission reduction, since it has a global effect with massive impacts. However, air pollution only involves few services we get from the ecosystem such as air quality and non-renewable sources while neglecting other relevant ecosystem services. Moreover, in the fast large scale implementation of new technologies like electric vehicles, there is remediation on air quality, with immediate positive health effects, but there is no guarantee on an improvement of other ecosystem services, and some others are heavily deteriorated.

This uncertainty calls for the development and improvement of all the available technologies, including the internal combustion engine platform which will require the integration with mitigation and remediation strategies to reduce the overall impact on the environment and to amend the damage already done, while keeping our economical and social structures.

One of the pillars for environmental impact mitigation is the use of emission

after-treatment systems where different catalysts are integrated in a sophisticated control system for minimizing harmful emissions. These after-treatment systems are transforming in a very dynamic and fast pace since new legislation towards tighter emissions is being introduced and reducing CO_2 emissions by fuel efficiency can increase other pollutants such as NO_x. Therefore, research on understanding the catalysts involved in the after-treatment system, specially the Selective catalytic reduction (SCR) catalyst, by the development of mechanistic models plays an important role in a sustainable transportation road-map where the internal combustion engine is still relevant.

1.2 A new approach for kinetic modeling

A kinetic modeling process involves multiple steps starting from the experimental design, parameter estimation and model validation, and ending in model deployment, where the model is used for what the modeling process it was intended. Most of the times this is a continuous, dynamic and ceaseless process, where the model evolves at each iteration. All of these steps require a multidisciplinary approach, and expert knowledge about catalyst and statistics, and well-defined expectations on the obtained model. A model is the utmost result of the scientific method, since it is a form of a highly complex hypothesis illustrated quantitatively and with physical significance when the model is mechanistic.

Kinetic modeling is usually focused on the parameter estimation process, where the optimal set of parameters is found for an assumed model structure by using an objective function. The model structure is taken from previous studies but most of the times there is no comprehensive model discrimination process. Models, as hypothesis, need to be evaluated among a defined set of candidates, so the best one can be selected by statistical criteria. The selection of a single model or small set of model candidates, is a big assumption on model development which is done frequently.

On the other side, the creation of feasible model structures involves expertise, and some imagination and inspiration. As Karl Popper stated, models are "the free creation of our minds, the result of an almost poetic intuition" [3]. Therefore, even if model specification can be conceptually hard, and sometimes subjective, it can benefit from the current advances on data science and computational tools.

Furthermore, complex models and high-throughput model discrimination require experimental data with high diversity. This involves exploding experimental regions for capturing relevant features. The experimental data need to be free from systematic artifacts which are present in real experimental setups. These artifacts have a significant effect on models since they provide wrong information for the inferences on the model and they add additional noise in the data which makes convergence harder in a non-linear model.

The expectation on the kinetic modeling process relies on finding a model which can approximate the data and can be generalized with available theories. This is a challenge, since it involves the relationship between phenomena at molecular level and the observations captured at a macroscopic level. As a result, an optimal compromise in the simplification of reality is needed for achieving understanding of the dominant features of the catalytic system with some error tolerances. Future work is certainly required for emission after-treatment systems to bring the new advances in computational tools and data science for closing the gap between the massive amount of information at molecular level and the model development process, bringing science utilisation.

1.3 Objectives

The objective of this thesis is to investigate and develop new experimental methods on gas flow reactors used in automotive emission after-treatment systems, for the development of kinetic mechanistic models in a data-driven modeling process. The development of an NH_3 adsorption model for a vanadium-based SCR catalyst was obtained by the development of an NH_3 adsorption experimental plan, a data pre-processing method for the characterization of the gas flow reactor, the quantification of artifacts, and a data-driven modeling process, where multiple adsorption model candidates were evaluated by a systematic process with some advances on data science and statistical methods.

In **Paper A** an experimental method for obtaining NH_3 adsorption data using a gas flow and a data pre-processing method for obtaining high resolution adsorption isotherms over a wide experimental region and from different samples is developed. The data processing method involves the characterization of the gas flow reactor by using a Residence Time distribution (RTD) model,

and the identification of systematic artifacts. This results in high resolution, repeatable data suitable for modeling purposes.

Then, in **Paper B**, a data-driven modeling process is developed involving multiple features. First a model structure generator was developed for creating multiple feasible model candidates by assuming the number of adsorption sites over a catalyst and assigning an adsorption mechanism from a previously defined database. Then, a sequential process with different objective functions for parameter estimation is proposed, which helps finding the optimal set of parameters by controlled and constrained steps. Finally, a cross-validation method is performed for obtaining robust parameters, and a quality assessment is implemented for evaluating the model in terms of fitting performance and overfitting.

This thesis aims to propose a systematic method for efficient model development for emission after-treatment catalysts, through the design of experiments maximizing the amount of usable information and by the selection of the best model with the use of computational tools, statistical methods and new data science techniques.

1.4 Thesis outline

The outline of this thesis is as follows:

- **Chapter 2** provides a background about the relevance of this project in the transportation sector, its relation with current and future legislation and the benefits on improving the after-treatment system. It also provides an overview about the vanadium-based SCR catalyst with the current proposed reaction mechanisms and kinetic models as well as the results from different experiments and DFT computations at molecular level. Finally, it provides a introduction on adsorption models, how the parameter estimation is performed focusing on the Akaike Information Criteria (AIC).

- In **Chapter 3**, a description of the experimental method developed for obtaining the data for the NH_3 isotherms over a wide experimental region is explained with the proposed data pre-processing method.

- **Chapter 4** outlines the data-driven modeling process for obtaining an

NH_3 adsorption model for the vanadium-based SCR catalyst by implementing some techniques on data science and statistics.

- In **Chapter 5**, the main results from the experiment for obtaining the NH_3 adsorption isotherms and from the modeling process where a mechanistic robust model with physical significance is presented. Moreover, a discussion about the advantages and challenges of the developed experimental method and modeling process is presented.
- Finally, in **Chapter 6**, the conclusions about the proposed methods and the obtained model are summarized with some remarks about the future work.

CHAPTER 2

Background

The section below provides the background for understanding the current project on NH_3 adsorption modeling on a vanadium-based SCR catalyst commonly used in diesel combustion engines. First, it provides an overview of the transportation sector, illustrating its size, complexity and the importance on reducing its environmental impact. The latter has been reduced by emission standards and the need of an emission after-treatment system, which is to increase its complexity in the future legislation. Then, an overview of the current emission after-treatment system is presented, focusing on the vanadium-based SCR catalyst, its proposed kinetic models and reaction mechanisms for NO_x reduction. Finally, an outline of the model development process, especially for the adsorption phenomena is presented, where different strategies for model building, parameter estimation and model discrimination are introduced. This includes the Akaike Information Criteria (AIC), one of the main elements used in the model development process in this project.

2.1 The transportation sector

The transportation sector is one of the main drivers of our society. It allows the movement of people and goods across the world, and it is involved in our daily activities. This sector supports globalization where raw material, production, and commercialization are decentralized [4]. As a result of its size and importance, it is not a surprise that transportation has one of the biggest environmental and energy impacts. For instance, it accounts for around 30% of the global primary energy consumption, and around 50% of the diesel global demand [5], [6]. Moreover, the transportation sector is estimated to produce around 30% of the global greenhouse gases (GHG) emitted [7].

One of the explanations for this impact is the sector's size. In 2015, the global fleet was estimated at 24 million trucks and 32 million vehicles used for public transportation and distribution [4], [8]. The largest fleet belongs to China, followed by the European Union, and USA. Furthermore, the annual sales in 2015 were around 100,000 trucks in Europe and around 139,000 in USA [4], [8]. Another explanation is the sector's diversity. The environmental impact is higher in developing and poor countries, since access to new technologies is sparse, there is lack of maintenance, and a backlog of older-vehicles with deficient emission after-treatment systems is persistent [9]. In fact, the average age for discarding a truck is higher in developing regions (around 25 years compared to 13 years in the European Union). As a consequence, a second hand market lies between developed and developing regions. For instance, used trucks from USA are sold in Mexico, and used trucks from the European Union are sold in Africa and Middle East [4], [9].

The environmental impact is mostly non-renewable resources' depletion and air pollution. Air pollution is defined as the negative effect caused by the concentration of pollutants in the air. The pollutants can have a local or wider effect, and the effect span can be minutes to years [10]. Air pollution is seen as an urban issue where there is a high vehicle density. The mix and severity of pollutants varies across the cities, since dispersion and concentration depend on weather, topography, emission sources, etc [5], [11]. Air pollution is a global problem causing 6.5 million deaths each year [10], [11]. In this regard the transportation sector is estimated to produce half of the global NO_x emissions (56 Mton), around 12% of sulfur oxides (SO_2), and 7% of particle matter (PM) [4]. However, even if the transportation sector is growing every year by 2.5%, NO_x emissions are being reduced by 10% and particle matter (PM) by 7%

due to the current emission legislation and after-treatment system [9], [12]. This trend in emissions reduction and sector growth is illustrated in Fig. 2.1.

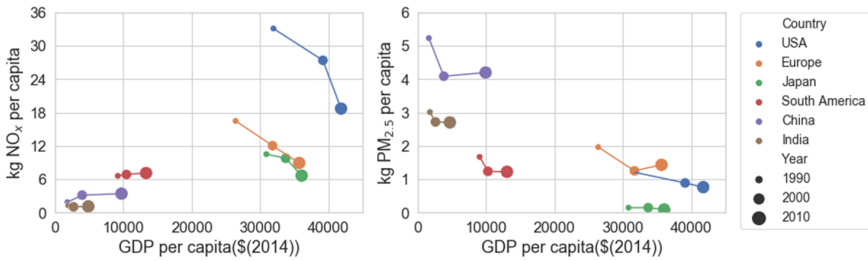

Figure 2.1: Emissions development at different countries/regions from different years or Gross domestic product (GDP) as an indicator of economic growth [10], [13]

.

Nowadays, the transportation sector's impact is increasing due to the continuous growth in commerce and public transportation, even with a disruptive event such as the COVID-19 pandemic, which gives uncertainty on future trends [14]. During the COVID-19 pandemic, emissions have increased since there was a boost on freight transportation due to e-commerce and use of personal car to avoid public transportation. However, the long term effects are still unknown [14].

In terms of environmental mitigation, the transportation sector is one of the most difficult sectors to decarbonize due to its diversity and magnitude [9]. Furthermore, this sector relies heavily on liquid fossil fuels since they have high energy density and the ease to supply with an existing infrastructure built since 1950's [8], [9]. However, the diversity can also help on finding tailored solutions where policies and technology are integrated. For instance, public transportation and last-mile distribution can be electrified with charging in centralized hubs [4].

Despite this, long-haul vehicles are even more complicated to decarbonize since there is a lack of technology and infrastructure [4], [6]. As a result, long-haul vehicles are estimated to rely on liquid fuels, fossil or from renewable sources, in the mid-term, increasing oil demand by 40% in 2040. This liquid fuel need impacts the strategy in the transportation sector for the future, aiming for the electrification of small vehicles, while keeping the liquid fuels to

the hardest transportation categories to decarbonize [4], [5], [9]. Nevertheless, this is an opportunity for increasing the biofuels supply and the development of new technologies for synthetic fuels [9].

Current legislation

Emission legislation is defined by each region or country. In particular, USA and European legislation have the most stringent legislation and they are used as reference to other regions such as China, India, and South America [4], [15]. Emission legislation has evolved at a very fast pace towards stricter limits and more robust protocols. As a result, emission control is an increasing expense on the total vehicle cost. For instance, while an emission control system costed around $400 for Euro II, it can cost around $7000 for the current Euro VI [16], [17].

In USA, the first emission legislation for heavy-duty vehicles was issued in 1974 for NO_x and particle matter (PM), and its application was voluntary [15]. Since then, legislation has evolved, being mandatory, and considering multiple pollutants with different inspection and system level. The legislation at federal level is issued by the Environmental Protection Agency (EPA), while for California it is issued by The California Air Resources Board (CARB) [12], [18]. Both regulations were aligned until 2007 when CARB decided for more stricter and faster implemented legislation [15], [16].

Nowadays, EPA and CARB have different perspectives. In 2020, EPA defined the Cleaner Truck Initiative aimed for lower NO_x emissions, and focusing on real conditions [4], [18]. However, in the last government, the initiative was classified as low priority and the implementation dates were moved in the future [16]. On the other side, CARB decided to adopt a new emission regulation in August 2020, setting NO_x limits for 2024 and 2027, introducing a new low load cycle, and extending system durability [12]. For instance, in the new CARB legislation, the useful life time is set at 800,000 miles, 12 years or 40,000 operating hours, and NO_x idling emissions are defined at 19 g/hour for 2024-2026 period and 5g/hour for 2027 and later [12], [15]. Another significant aspect of the emission legislation in USA is that it is complemented with fuel economy and GHG emission reduction standards since 2017 [9], [12], [15].

In the case of Europe, Euro I standard was adopted in 1991 for heavy-duty vehicles and buses [15]. It evolved to the current Euro VI standard which was

introduced in 2009 and became effective in 2014 [4], [16]. This standard is extended to different combustion engine platforms such as compression ignition, positive ignition and dual fuel engines [15]. The Euro VI standard established requirements for Particles Number (PN) and On-Board Diagnostics (OBD), in-service conformity testing, and a limit for NH_3 of 10 ppm during all the test cycles [16], [17]. Furthermore, the durability requirement was defined at 700,000 km or 7 years [19], [20].

The Euro VI standard and future ones, are aimed to be integrated with a GHG emission regulation, which was first introduced in 2019 [15]. The GHG standard applies to multiple sectors, including the transportation sector, and it aims to reduce GHG emissions by 15% in 2025 and 30% in 2030, using measurements from 2019/2020 as reference [9], [20]. The standard focuses on tank to wheel CO_2 emissions, and has a manufacturer fleet basis strategy, where the average CO_2 emissions for the overall fleet is calculated by standardized simulations [15]. As a result, this legislation suggests the implementation of technologies such as batteries or hydrogen to be able to comply by 2030 requirements [9], [21].

Fig. 2.2 shows the evolution on emission limits set by legislation on truck for different countries for NO_x and PM [4], [16].

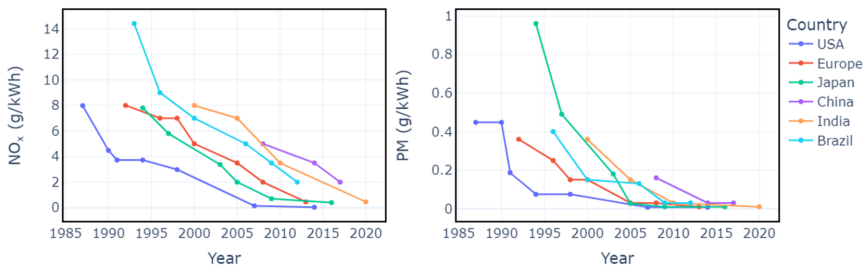

Figure 2.2: Emission limits for heavy-duty vehicles for NO_x and PM for different countries from 1985 to 2020 [4], [16].

The emission limits illustrated in Fig. 2.2, are evaluated by standard cycles, where results can be replicated across different stakeholders, providing comparisons between different brands, technologies, conditions, etc [15]. A standard cycle tries to compile the most important features on typical driving conditions is USA, Europe, Japan, etc [15], [22]. The two most commonly

used cycles are explained in Table 2.1

World Harmonized stationary cycle (WHSC)	World Harmonized transient cycle (WHTC)
• Sequence of steady-state engine modes with specific torque and speed. Duration: 1895s • Loads vary between 25% to 100% rated (4 load points). • Speeds vary between 25% to 75% rated (6 speed points).	• World-wide real driving pattern for heavy-duty transport. • Duration: 1800s. It is divided into an urban (900s), rural (468s) and highway (432s) part.

Table 2.1: Standard cycles for testing emission levels [15], [22].

Future legislation proposals

Euro VII and CARB 24-27 standards have been considered in the last years, trying to reach an agreement between the different stakeholders as well as pushing emission limits to the lowest possible value considering technical constraints in catalysts, sensors, controls, etc [16], [19], [20]. Both future standards, Euro VII and CARB 27, are aimed to be fuel and technology neutral, with a holistic approach where the entire life cycle on fuel supply is analyzed (well to wheel) [17], [19]. This will give opportunities to multiple technologies to develop, not only the most favorable nowadays [9], [20]. In the future standards, the main challenge is to reduce NO_x levels without increasing GHG emissions or fuel consumption, and meeting the emission limits at multiple driving and environment conditions for the product life time [17], [22].

Current criticism in the proposals for Euro VII and CARB 27 are concentrated on the clear preference for electric vehicles by proposing emission limits and protocols difficult to achieve by the current technology [4], [17], [23]. Moreover, an environmental legislation should involve other types of impacts besides air quality [24]. The proposed approach in the regulations does not consider the transition in transportation as the continuous improvement of the current technologies such as the internal combustion engine [17]. This improvement includes higher efficiencies, the use of alternative fuels, and the investment on remediation processes such as carbon capture to mitigate GHG emissions from the sector [17], [23].

In Europe, during the last two years, the European Commission designated a technical group, AGVES, to propose feasible emission limits for the Euro VII standard [22]. Based on multiple studies from different stakeholders, their proposal aims to reduce emissions by more than 80% on most pollutants while including new pollutants to monitor as presented in Table 2.2 [22]. Furthermore, the Euro VII proposal is boosted by the European Green Deal, designed to accelerate the shift to sustainable and smart mobility, with stricter regulations and the implementation of new technologies for renewable fuels [19], [20].

		Euro VI	Euro VII			
		WHTC (combined)	WHTC Cold	WHTC hot	Combined WHTC Euro VI method	New combined scenario
NO_x	*mg/kWh*	460	210	45	68	40
PN	*1/kWh*	6E+11	3E+11	5E+10	9E+10	1E+11
CO	*mg/kWh*	4000	2600	27	387	400
NMHC	*mg/kWh*	160	120	14	29	50
NH_3	*mg/kWh*	80 (10ppm)	50	36	38	10
N_2O	*mg/kWh*	None	136	45	58	25
CH_4	*mg/kWh*	500	430	135	176	50

Table 2.2: Proposed emission limits for Euro VII by AGVES [22].

These new proposals point the need for developing new measurement methods and robust protocols for certification at real conditions [19], [20]. Moreover, they add pollutants such as NH_3, CH_4, N_2O, aldehydes and volatile organic compounds (VOCs) to be regulated at all technology platforms, while NO_2 is separated from NO_x emissions [16], [22]. The proposed emission limits are applied to all operating modes including DPF regeneration, and idling, with a focus on low temperature and urban cycles, since they have the highest impact on emissions [19], [22]. Another feature of the future standards is the market surveillance program for fleet screening and open access data [19], [22].

Difficulties arise in the implementation of new technologies and effective regulations due to how the market is established. From a business perspective, the use of new technologies depends on the payback gap, how the investment is fully amortized by operating savings, and the access to capital for large scale investment for infrastructure [4], [16]. However, carriers and companies

in transportation are focused on surviving in a competitive market and sustainability is in some cases driven as a publicity boost [20]. To solve this issue, the majority of stakeholders in transportation have suggested the need for investment in the following areas for a better integration between technology and regulation, with collaboration between companies, government and academia [4], [20], [21].

- Improvement on the business model: This does not involve technology advances but a change on the business model for meeting customer demands while minimizing resources. The improvements involves increasing the road quality, creation of logistic hubs, and increasing the collaboration between companies and logistic projects.
- Improvements on fuel efficiency: This requires the investment on technologies with lower payback periods or an appropriate incentive for implementation.
- Use of alternative fuels: This includes solving the dependency on fossil fuels or other non-renewable sources. Moreover, it requires the implementation of a decarbonization strategy including mitigation, and the development of methods for evaluating impact on all the production levels, including recycling. Additionally, this involves the investment in multiple technologies such as natural gas, biofuels, hydrogen and electricity. [4], [16], [21]

Future emission after-treatment configurations

Different prototypes have been developed for evaluating the expected performance of the current state-of-the-art emission after-treatment system for defining the emission limits for Euro VII and CARB 27 standards. It is expected that the emission after-treatment system price will increase between $2000 to $5000 [12], [16]. For the Euro VII standard, the proposed configurations by AGVES are presented in Fig. 2.3 [17], [19], [22].

The proposed configurations require a close-coupled system for reducing emissions at cold-start. For a robust control, a heated dosing system or an electrical catalyst heater (ECH) is suggested that can lower the dosing temperature to 130°C. As the emission after-treatment system is heated, there is a transition towards the underfloor SCR catalyst, since NO_x need to reach the

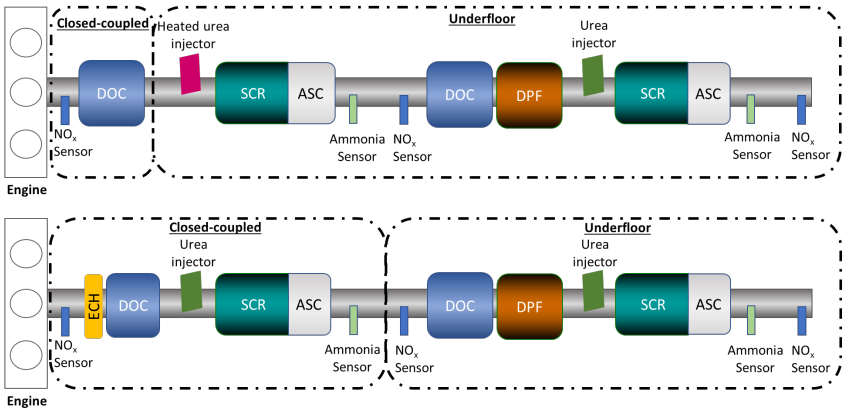

Figure 2.3: Proposed emissions after-treatment systems for Euro VII standard by AGVES [22]

.

DPF for NO_2 formation and passive regeneration [22]. At high temperatures the closed-couple system usage is reduced, but as temperature decreases, the NH_3 coverage is restored to be prepared for the low-temperature transient [17], [22].

The underfloor system considers a standard configuration from the Euro VI standard (DOC, DPF, SCR and ASC catalysts), which is suitable for high speed/load driving conditions [22]. The proposed configurations also suggest multiple NO_x and NH_3 sensors for tighter control on NO_x reduction and urea injection, reducing side reactions. On the engine side, the main goal is to reach high temperatures faster, higher than 200°C, in the after-treatment system without fuel penalty [17], [22].

The proposal for CARB 27 is shown in Fig. 2.4. This configuration is similar to the one suggested for Euro VII standard. However, in CARB 27, a dual SCR catalyst and a Catalytic soot filter (CSF) with DOC and DPF functions is suggested [25], [26]. Furthermore, more NH_3 and NO_x sensors are required for the implementation of a model-based SCR control with real time feedback control and regulation of the NH_3 storage capacity [27]. The proposed engine configuration involves engine gas recirculation (EGR) and cylinder deactivation, where the number of cylinders can be chosen based on operating conditions, reducing the GHG emissions at low loads [25].

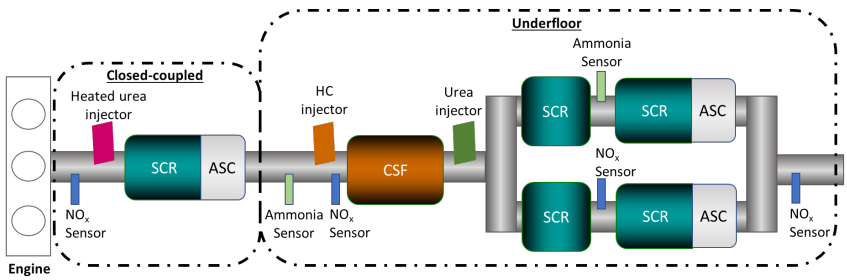

Figure 2.4: Proposed emissions after-treatment system for CARB 27 [25].

As explained earlier, the control system for the future emission after-treatment system needs to be model-based, for estimating the NH_3 coverage on the different SCR catalysts in the system [27]. The proposed model is a tank-in-series model for estimating the total NH_3 coverage as well as the axial distribution. The control system involves short and long term feedback elements [27]. The NH_3 sensors are used for the short term feedback, while the NO_x sensors are used for the long term feedback [25], [27]. Both loops combined, balance the NH_3 load, improving SCR catalyst conversion, reducing the NO_x and NH_3 peaks during transient operation, and minimizing side reactions [27]. Moreover, the model-based control can include parameters for aging. The proposed control system scheme is presented in Fig. 2.5.

2.2 The emission after-treatment system

Emissions are formed as a product from combustion of the fuel in the engine, producing gases such as CO_2, NO_x, H_2O, CO, soot and partially combusted hydrocarbons [28]. The reduction of these emissions is required by legislation since these pollutants have an impact in the environment and human health. Emission reduction is done with two main strategies: engine optimization, where the fuel consumption is minimized and therefore the amount of pollutants, and emissions treatment through the use of a catalytic module [28]–[30]. The emission after-treatment system has several functions and catalysts with different functionalities are used. The optimization and synergy among the catalysts is key for reducing pollutants in a wide range of operating conditions and minimum volume [31]. A heavy-duty Euro VI after-treatment system is

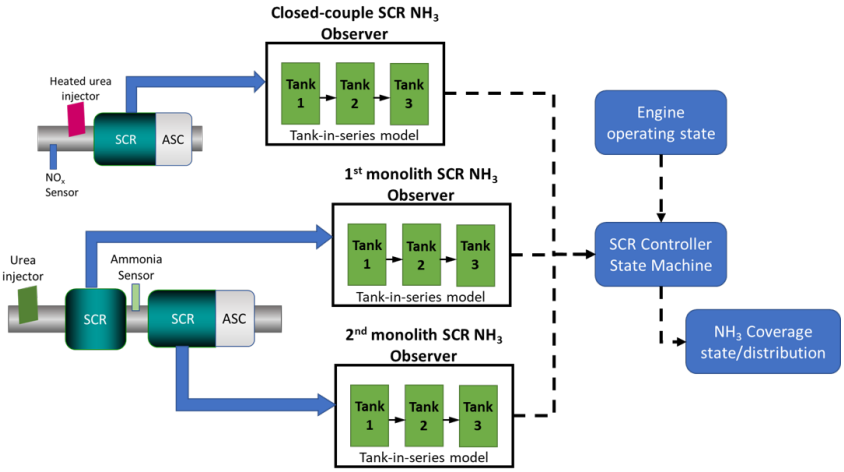

Figure 2.5: Proposed NH_3 model-based control system for CARB 27 [27]

.

illustrated in Fig 2.6 [32]. The main components are:

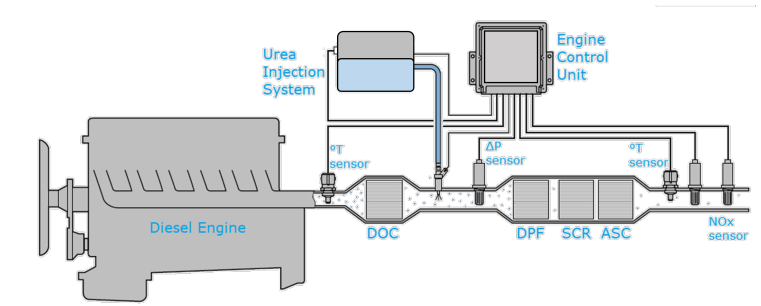

Figure 2.6: Typical Euro VI exhaust emission after-treatment system for a diesel engine [32].

- DOC (Diesel oxidation catalyst): Oxidizes partially combusted hydrocarbons and NO_x to NO_2 to increase low-temperature conversion for the SCR catalyst.
- DPF (Diesel particulate filter): Removes soot particles that are oxi-

dized with an active (temperature increase) or passive (catalytic coating) method.

- Urea injection: An injection system for Adblue® (a water solution of 32.5% urea) is the source of NH_3 as the reducing agent in the SCR catalyst.

- SCR (Selective catalytic reduction) catalyst: Reduces NO_x into N_2 and H_2O using NH_3.

- ASC (Ammonia slip catalyst): Oxidises the NH_3 excess that is not converted in the SCR.

- Sensors: The after-treatment system needs several sensors for appropriate control. A NO_x sensor is required downstream the system for monitoring NO_x and NH_3 and regulating urea injection [30]. A temperature sensor is installed since catalyst performance is affected by the temperature of the system. Moreover, a differential pressure sensor is installed in the DPF for monitoring pressure drop due to soot and ash build-up in the filter which affects engine efficiency.

The SCR catalyst is the key component for NO_x reduction, which proceeds in an oxidative environment (lean), with the use of a reducing agent such as NH_3 and a catalyst to increase selectivity and the reaction rate [29], [33]. However, a proper control strategy, with an optimal supply of NH_3 is required because an excess of NH_3 could increase urea consumption, and it could produce side reactions towards N_2O, a potent greenhouse gas [34]. The current after-treatment systems do not provide a way to reduce N_2O emissions [32].

The vanadium-SCR catalyst

Nowadays, vanadium-based and Cu-zeolites are the most common catalyst used in a single or combined configuration for NO_x emissions abatement. The vanadium-based SCR catalyst has been used since 1970s in power plants and was extended to the automotive industry in the 1990s for diesel engines [35]. The vanadium-based SCR catalyst provides high conversion in a temperature range of 300 to 450°C, with poisoning resistance against sulfur and some alkali-metals [29], [36], [37]. The catalyst surface has different vanadium structures

which are highly dynamic. For a vanadium-based SCR catalyst, the vanadium concentrations are low: between 3-7 weight% below the monolayer limit concentration [38], [39]. Increasing the vanadium concentration lowers the N_2 selectivity towards N_2O. The distribution below monolayer is stable on reducing, oxidizing and reaction environments [38], [40], [41].

In an after-treatment system, the catalyst is a honeycombed monolith since they provide low pressure drop, high mechanical strength, low tendency for clogging and high surface area for active sites [28], [31]. The catalyst can be extruded or washcoated. For the extruded catalyst, the active material with the support and promoters is extruded in a single piece. For the waschcoated catalyst, a substrate (ceramic or metallic) is built where the active material and promoters are added forming an external layer with a defined thickness [29], [42].

For vanadium-based SCR catalyst, TiO_2 in anatase form is found to be the best support since the activity is enhanced due to hydrogen mobility and is weakly affected by sulfur. The anatase TiO_2 has higher surface area (50-80 m^2/g) and it is thermally stable at 500°C [38], [41]. However, at higher temperatures the anatase is transformed to rutile, with a lower surface area (<10 m^2/g), affecting the catalyst activity due to structure collapse [29], [38]. Tungsten (W) is added as promoter since it increases the surface acidity, favors NH_3 storage, promotes faster water desorption, and delay sintering due to thermal aging [39], [43]. Moreover, tungsten is a competitor for active sites, making the vanadium aggregates closer together and affecting its structure, which increases the SCR activity and broadens the operational temperature range [38], [43]. The effect of promoters is stronger in polymeric vanadium structures [39], [44].

In reducing environments the vanadium oxidation state changes from +5 to +4 and +3, with the polymeric vanadium species easier to reduce than the monomeric species [38], [41]. By contrast, the TiO_2 support is not reduced. At dehydrated conditions with oxygen, water desorbs from the catalyst surface and vanadium reaches its highest oxidation state [38], [39]. The different vanadium species, monomeric and polymeric, have well defined structures. When water is added at high temperatures, the vanadium keeps its structure and a hydrogen bond is formed between H_2O and the V=O, increasing the Brønsted acidity. At low temperatures, water forms a monolayer blocking the vanadium sites [37], [40], [44], [45].

Another significant aspect of the vanadium-based SCR catalyst is its robustness against chemical poisoning [29]. However, some contaminants have an effect on reducing the activity or increasing the reaction rate of undesirable reactions. Phosphorous (P) can bind to the vanadium site, while compounds such as Ca, Zn, K, and S reduce the amount of active sites due to pore blocking [46], [47]. Vanadium-based SCR catalysts are more sensitive to thermal aging than the Cu-zeolite SCR catalyst, since the anatase is transformed to rutile and vanadium starts to sublimate being a health and environmental risk [48], [49]. Therefore, a reliable thermal control system is required, where active DPF regeneration is not recommended.

SCR Mechanism and kinetics

Several kinetic studies have been carried out for the vanadium-based SCR catalyst under different conditions since it is important to understand the reaction mechanism over a wide operating region for automotive applications. The simplest kinetic model is a power law kinetic, for the overall SCR mechanism [50]. Nevertheless, this simple model already provides information on the interactions of the different compounds over the catalyst surface [51]. For a vanadium-SCR catalyst, the NO_x conversion power law kinetic model is presented in Eq. 2.1 [50], [51].

$$\begin{aligned} \text{Overall SCR} \quad & 4\,NO + 4NH_3 + O_2 \longrightarrow 4\,N_2 + 6\,H_2O \\ & r_{NO} = A e^{-\frac{E_{act}}{RT}} [NO]^{\alpha} [O_2]^{\beta} [NH_3]^{\lambda} [H_2O]^{\delta} \end{aligned} \tag{2.1}$$

Where, A is the pre-exponential factor, E_{act} is the activation energy, and α, β, λ and δ are the reaction orders for NO, O_2, NH_3 and H_2O, respectively. For the vanadium-based SCR catalyst the activation energy and reaction orders are shown in Table 2.3.

	α	β	λ	δ	E_a **(kJ/mol)**	Ref.
$\mathbf{V_2O_5/TiO_2}$	0.5 - 1.0	0.2 - 0.5	0 - 1[a]	-0.10 - -0.14	41 - 50	[50]–[52]
[a] $\lambda = 0$ at high concentrations, $\lambda = 1$ at low concentrations or low NH_3 / NO ratios.						

Table 2.3: Reaction orders for the NO conversion rate power law kinetics for the vanadium-based SCR.

The reaction order for O_2 is usually zero since it is in excess at normal oper-

ating conditions. However, oxidation plays a role in the catalyst re-oxidation, which gives a positive reaction order and it can be limiting at certain conditions [51], [53]. The reaction order for NH_3 depends on the NH_3 gas concentration and temperature. At high concentrations the reaction order is zero since the maximum NH_3 adsorption capacity is reached faster in a vanadium-based SCR catalyst. NH_3 is strongly adsorbed in the surface, and it requires to be activated, limiting the reaction rate, with a reaction order of 1 at low concentrations [52]–[54]. The reaction order for H_2O is neglected at high concentrations but it can have negative reaction order, since there is a competition for adsorption sites with NH_3, but it improves selectivity at lower temperatures. The reaction order for NO is positive but it is conditioned by the NH_3 concentration and side reactions [53], [55]. Finally, it is found that the activation energy depends on the preparation method, ranging from 41 to 50 kJ/mol [51], [53].

A global mechanism involving the different reactions over the vanadium-based SCR catalyst has been a challenge due to the diversity of species over the catalyst surface, and the wide operating region in an automotive application [45]. The most common mechanism proposed is where NH_3 is strongly adsorbed and reacts with gaseous or weakly adsorbed NO [37], [45], [56]. NH_3 adsorbs on the vanadium, as the active site, and the tungsten and the support as reservoirs [44]. For reaction, NH_3 adsorbs on Brønsted vanadium acid site and it is activated by an adjacent vanadium redox site. The activated NH_3 reacts with NO, producing N_2 and H_2O, and partially reducing the active vanadium site [39], [57]. The reduced site is regenerated by oxygen. This mechanism, shown in Fig. 2.7, was proposed by Topsoe at al. [44], [56], and it is the basis for more complex mechanisms. From their experiments, they found that the SCR reaction is the limiting step at high O_2 concentrations, while NH_3 adsorption is the limiting step at low NH_3 gas concentrations [56]. Arnorson et al. [58], complemented the SCR mechanism proposed by Topsoe by considering the standard and fast SCR in a two-cycle mechanism. The cycles differ in the NO activation step, for the standard and slow SCR. They share the same reduction step, but for re-oxidation, the standard SCR mechanism uses NO + O_2 and the fast SCR uses NO_2. The proposed mechanism is shown in Fig. 2.8 [58], [59].

Lian et al. [60], found that polymeric vanadium species have a higher activity than monomeric vanadium species since closer adjacent species reduce the

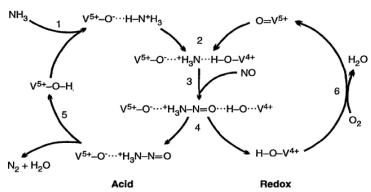

Figure 2.7: Standard SCR mechanism proposed by Topsoe et al. Taken from [56].

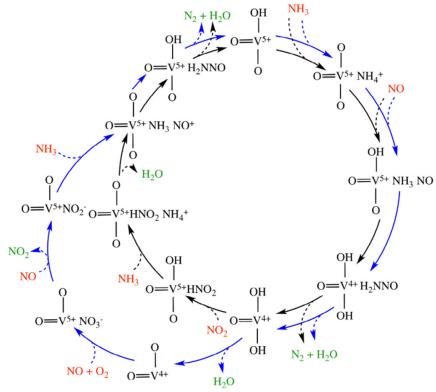

Figure 2.8: Two-cycles SCR mechanism proposed by Arnarson et al. Taken from [58], [59].

reaction pathway for regeneration hence increasing the SCR activity. They proposed two SCR mechanisms with an active role of the TiO_2 support where NH_3 can adsorb and play a role for NO_x activation [61]. The reaction mechanism for the monomeric and polymeric vanadium species is presented in Fig. 2.9 [60].

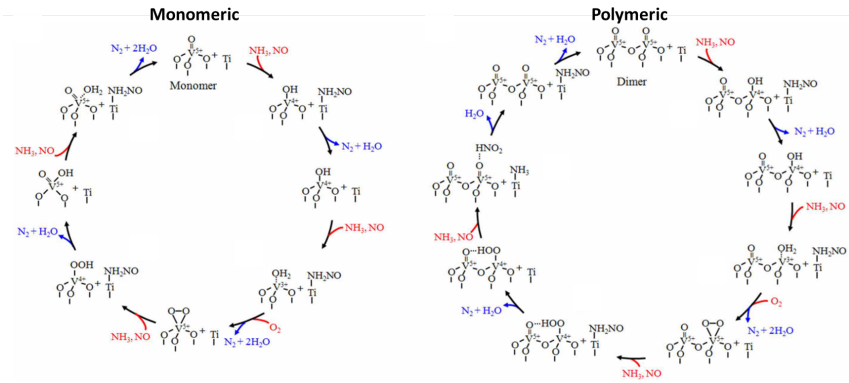

Figure 2.9: SCR mechanism for a monomer and dimer vanadium over a TiO_2 surface. Taken from [60].

For the proper kinetic modeling of the SCR mechanism, there are some challenges still being investigated: the molecular nature of the NH_3 adsorption/desorption on Lewis and Brønsted sites and its behavior at different temperatures and gas concentrations, the consumption and regeneration of active sites under different conditions, and the rate determining step in the SCR redox cycle [34], [36], [44]. Furthermore, the role of compounds such as H_2O, O_2, NO_2, and the formation of intermediates towards new reaction pathways such as the nitrates also calls for further research [33], [35].

Summarizing the SCR mechanism into a kinetic model is a complex task since there are multiple variables to consider with a highly non-linear behavior. The overall SCR global kinetic model commonly used is the Eley-Rideal mechanism, where NH_3 is strongly adsorbed on a Brønsted acid site $V^{+5}-OH$, and the NO is weakly adsorbed or in gas phase for reaction [56], [62]. The Eley-Rideal mechanism does not include the re-oxidation step but it can be complemented by a Mars-Van Krevelen mechanism including the redox mechanism, where oxygen plays a role in the reoxidation of vanadium sites, being a limiting step at high temperatures [34], [63]. However, in most of the operating cases, the influence of oxygen is neglected since the catalyst is operating at high O_2 concentrations [33], [37].

Tronconi et al. [36] proposed an improvement to the Eley-Rideal and Mars-van Krevelen kinetic models, by accounting for NH_3 inhibition at low temperatures, considering two main sites: one redox site and one acidic site. The redox site adsorbs O_2 and NO, and activates NH_3, while the acidic site is a reservoir for NH_3 adsorption. The O_2 dependence in the reoxidation is modelled as a power law relation for simplification. Later, Tronconi et al. [34], [62] proposed a complementary SCR model where NH_3 is not available. In this model, NO adsorbs on a vanadium site, forming a nitrate species. The nitrate species can be formed by NO or NO_2. Then, when NH_3 is available, nitrates form ammonium nitrate at low temperature which then decompose into N_2 and H_2O. At very low temperatures, the ammonium nitrates can block reaction sites, but it is reversible at high temperatures [36].

The proposed SCR kinetic models neglect the influence of NO_2 for the fast SCR reaction. In that regard, Ciardelli et al. [35], [62], proposed a reaction mechanism accounting for the influence of NO_2 which was integrated to the one formulated by Tronconi et al. The new kinetic model provides good results under transient conditions, since relevant features like NH_3 inhibition

at low temperature, NH_3 spillover from acid sites to redox sites, and the NH_3 adsorption on multiple sites are included [33], [35]. However, their results show deviations in the NH_3 gas outlet concentration that can be interpreted as lack-of-fit on the NH_3 storage estimation.

NH_3 Adsorption experiments and first-principle studies

The NH_3 adsorption over the vanadium-based SCR catalyst is important for the understanding of the SCR mechanism but it is still unclear due to the diversity of sites in the catalyst [64], [65]. NH_3 is believed to adsorb on two main sites: it molecularly adsorbs on a Lewis acid site with coordinate unsaturated cations, and it adsorbs as NH_4^+ on a Brønsted acid -OH site [39]. The Lewis acid sites contain an empty orbital to receive an electron pair. In the vanadium-based SCR it can be an element such as V, W or Ti double bonded with oxygen (M=O). The Brønsted acid site is able to release a proton and it has the structure in the form M-OH [39], [61].

NH_3 adsorption is different on the different vanadium species at the catalyst since it is affected by the oxygen atoms surrounding a vanadium atom and the structures formed by this interaction [66]. Different vanadium species capable for NH_3 adsorption have been identified: monomeric vanadium in a tetrahedral configuration attached to the support, 2-dimenssional polymeric octahedral clusters, where the dimer vanadium species is the smallest, and V_2O_5 clusters when the monolayer concentration is exceeded. Furthermore, using in situ IR, Wachs et al., identified Lewis sites in TiO_2, Brønsted and Lewis sites in vanadium, and Brønsted and Lewis sites in tungsten [39], [59], [67]. They also found that Lewis acid sites can be transformed into Brønsted acid sites, with water at high temperatures (>250°C) [66].

Topsoe et al. [39], found similar site diversity over the vanadium-based SCR catalyst, confirmed by the continuous release of NH_3 over a wide temperature range when TPD experiments were performed. They found a relevant role for TiO_2, since vanadium interacts with Ti-OH groups for NH_3 activation, and when the catalyst is fully reduced, NH_3 is still present on the support at higher temperatures (>300°C) [68], [69]. Since the Lewis acid sites have higher adsorption energies than the Brønsted acid sites, they have the main role in NH_3 adsorption at high temperatures.

Several first principles studies by density functional theory calculations have been performed for establishing the main steps in the SCR mechanism [70]–

[72]. Periodic models are more appropriate since they account for the diversity of the vanadium-based SCR catalyst. These studies provide a calculation for the adsorption enthalpy for NH_3 and water, for different species on the catalyst surface. The obtained adsorption enthalpies provide a reference for kinetic modeling. Fig. 2.10, shows the different adsorption enthalpies extracted from these studies including adsorption values for monomeric and polymeric vanadium, and the TiO_2 support [59], [67], [70], [73], [74]. Moreover, the interaction between vanadium and support, and defects on the catalytic surface is critical for increasing activity and promoting adsorption [38].

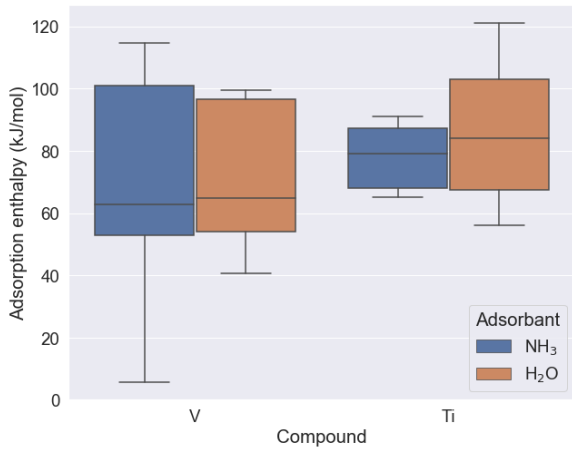

Figure 2.10: Enthalpy of adsorption for NH_3 and water over vanadium and titanium oxide clusters from different DFT studies [59], [67], [68], [70], [73]–[76].

For the monomeric vanadium species, NH_3 adsorbs on the V-OH adjacent to the TiO_2 support. A second NH_3 molecule, can adsorb between the vanadium and the adsorbed NH_4^+, with the N atom facing the nearest H atom from the NH_4^+ [59]. When the adjacent atom is a tungsten atom, the redox site becomes more active and adsorption is more feasible. Water can also adsorb in two configutations: to the exposed cation +5 and the -OH. If water is bonded to the O atom in the vanadium site, it dissociates [73]. When water dissociates, the OH^- species goes to the vanadium site while the H^+ species goes to the adjacent O atom [66], [70].

For the polymeric vanadium species, the adsorption energy decreases as the size of the site increases [68], [77]. Moreover, polymeric sites have exposed vanadium atoms which can act as Lewis sites since they can receive an electron pair from the nitrogen in NH_3. Hydroxyl species are formed over the vanadium species by dissociation of water. In the polymeric vanadium, there are three oxygen atoms which can be transformed to Brønsted acid sites after interaction with water [68], [69]. However, NH_3 adsorption is most favorable at the terminal O atoms since one proton interacts with the adjacent vanadyl oxygen and NH_3 donates its electrons to the TiO_2 support [72].

For the TiO_2 support, NH_3 can adsorb on two Lewis acid sites. NH_3 adsorbs via the N atom bonded to the Ti atom on the Lewis acid site. However, Lewis sites from the support or the vanadium site are hard to distinguish. For water, the adsorption enthalpies are lower than for NH_3 [74], [75]. Furthermore, the support can have Brønsted acid properties in the bond Ti-OH-Ti when a monomeric vanadium is close [73].

As a summary, the main vanadium structures present in the vanadium-based SCR catalyst onto which NH_3 and water can adsorb are illustrated in Fig. 2.11. Two main groups can be identified: monomeric and polymeric vanadium species, which interact with adjacent atoms such as tungsten (W) or titanium (Ti) to develop Brønsted and Lewis acid sites dynamically.

2.3 Towards a modeling framework

A true model, able to represent reality at its full extent, has infinite dimensions and it cannot be captured by limited observations from measurement devices with limited resolution [78]. The hope relies on finding the best model which could approximate and maximize the amount of information from data, with a generalization based on available scientific theories or knowledge [79], [80]. In a data-driven modeling approach, the best model is chosen from a set of several candidates. Each model is seen as a hypothesis, speculation or guess from previous knowledge and experiences that are evaluated by the experimental tests [81], [82]. Based on the evaluation of such models, it is possible to achieve understanding, supporting the model with experimental data and a physical explanation based on science [78].

Modeling involves two sequential processes: induction, where multiple models are specified using data and previous knowledge, and deduction where a

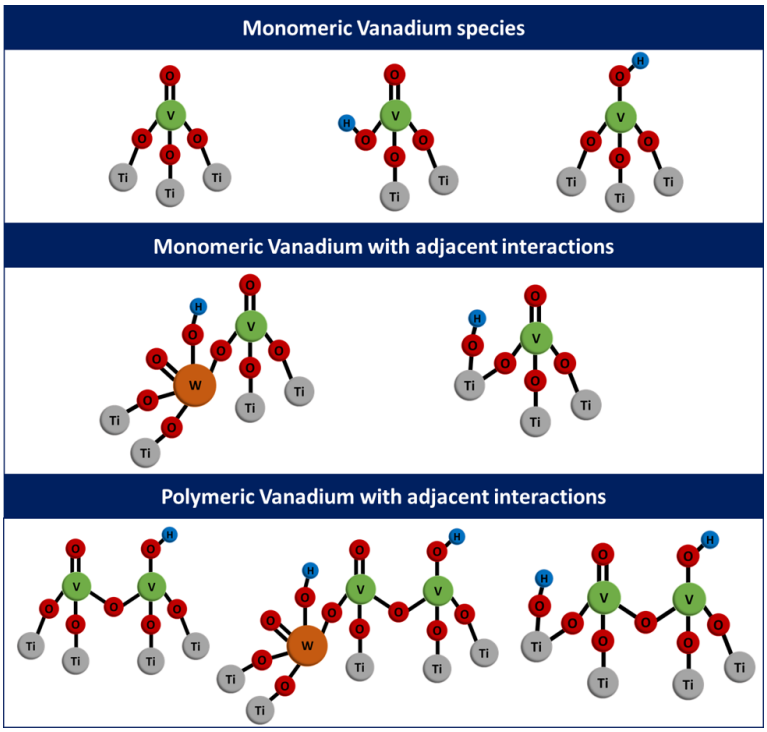

Figure 2.11: Multiple vanadium species present in vanadium-based SCR catalysts for NH_3 adsorption.

generalization of the desired phenomena is described by the model [81], [83]. In that way, inference by modeling involves a balance between prediction and explanation. Acceptable prediction performance is achievable by non-mechanistic models but mechanistic models provide a scientific explanation to complex hypotheses but they are more time consuming [78], [84]. A data-driven model development is an iterative process involving the following steps: formulation of a set of model candidates, experimental planning, data collection, data processing, model fitting, model verification and quality assessment [81], [85]. The iterative modeling process is shown in Fig. 2.12.

A preliminary analysis is required to formulate a set of feasible model candidates, supported by the current scientific knowledge [78], [86]. Moreover,

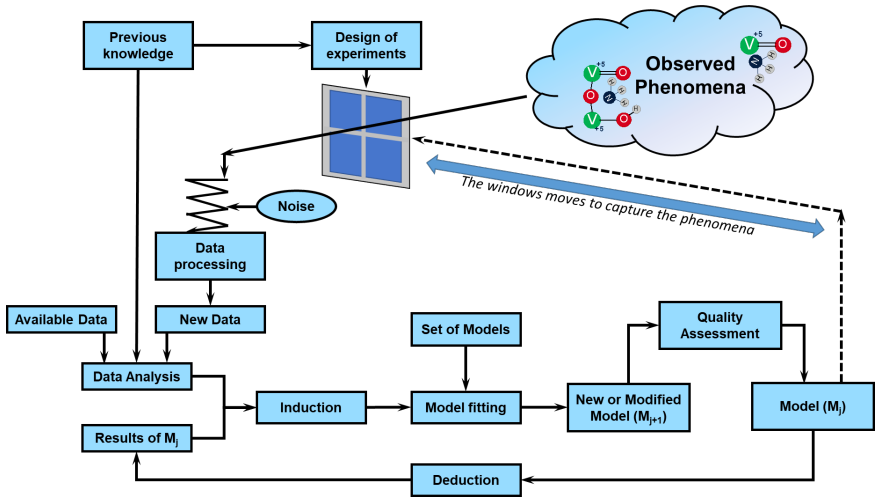

Figure 2.12: Model development process [81]

this analysis helps on identifying the key features to be exploited during the experiment for model identification and discrimination [81], [87]. During the experimental planning, one should aim to an experimental region able to discriminate between rival models and improvement of parameters' precision. Poorly planned experiments are a waste of time and resources, and the limited amount of data should aim to the maximization of information, minimizing the use of resources [87].

In an experimental plan, the controlled variables, initial conditions, time, pretreatment procedures, sampling times, and measured response times need to be identified and specified [78], [88]. Furthermore, systematic error sources should be identified and minimized or removed in a data processing step. Moreover, the random error from measurements should be normally distributed and low in magnitude compared to the measurement [89].

The data collection, processing and fitting involves the implementation of computational procedures based on statistics and optimization. These steps are iterative, where different approaches should be tested for model quality and robustness [81], [83], [88]. In most cases, it involves subjective choices which need to be stated and supported. For model fitting over a wide experimental region, there are different strategies such as the Bayesian model

averaging approach, or model segmentation where the parameter fitting is done on segmented data [78], [89].

Model verification and refinement involves different processes. The identification and removal of outliers, improves the parameters confidence interval and avoids reaching wrong conclusions based on the chosen model [87]. A sensitivity analysis evaluates how fluctuating are the conclusions reached by the model, and it can be done by evaluating the first-order response change of the expected value, when a parameter is modified within a margin [85], [89].

The models obtained in this iterative process should be able to separate information from noise [78], [90]. Additionally, they must be objective and repeatable. Furthermore, the models need to be simple, precise, with unbiased parameters and some indicators for precision. The model structure and parameters should have physical meaning supported by other independent experiments [80], [89].

Adsorption models and thermodynamic relation

An adsorption isotherm describes the equilibrium state of the adsorption and desorption rates for a gas compound in a dynamic balance with its adsorbate state over a catalytic surface [31], [91]. The equilibrium state is affected by temperature, gas concentration, and catalyst properties. Moreover, this state can be described by thermodynamics, in terms of the entalphy and entropy changes, ΔH and ΔS, providing insight on the adsorption strength and molecules' arrangement [91]. At equilibrium, an adsorption kinetics can be formulated as presented in Fig. 2.13.

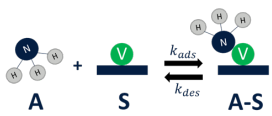

Adsorption kinetics

$$r_{ads} = k_{ads} C_A \theta_S$$

$$r_{des} = k_{des} \theta_A$$

$$k_i = k_i^o exp\left(\frac{-E_a}{RT}\right)$$

$$\theta_{Tot} = \theta_S + \theta_A = 1$$

At equilibrium

$$r_{ads} = r_{des}$$

$$\theta_A = K_c C_A \theta_S$$

$$K_c = \frac{k_{ads}}{k_{des}}$$

Figure 2.13: Adsorption kinetics and equilibrium model

In Fig. 2.13, the adsorption rate, r_{ads} depends on the gas concentration,

C_a, and the number of available free adsorption sites in the catalyst, θ_S, while the desorption rate, r_{des}, depends on the number of adsorption sites already occupied by the adsorbate, θ_A [31], [92]. The adsorption and desorption reaction rate constants, k_i, can be expressed following the Arrhenius equation with a temperature dependence on the activation energy [91]. For the NH_3 adsorption rate constant, k_{ads}, the activation energy over a vanadium-based SCR catalyst is assumed to be zero since it is non-activated and spontaneous [34], [93].

The activation energy for the desorption rate, can be estimated based on the adsorption model used. Several adsorption models have been evaluated in previous studies for NH_3 adsorption in vanadium-based SCR catalysts: Langmuir, Freundlich, Temkin and modified Temkin [93], [94]. Langmuir models assume homogeneity for the adsorption sites distributed over the catalyst surface, but other models try to include surface heterogeneity, by adding more sites or using empirical correlations [94], [95]. The main features about the existing adsorption models for NH_3 adsorption over vanadium-based SCR catalysts are explained below [31], [94], [96], [97]:

- Langmuir: In this model, the activation energy for desorption, E_d, is a constant. This model assumes monolayer adsorption on limited adsorption sites over the catalyst. The adsorption sites are identical and equivalent, with no interactions with adjacent species, and homogeneously distributed in the catalyst surface. The Langmuir model is consistent with Henry's law at low gas concentration and its parameters provide a mechanistic approach related to thermodynamic properties.

- Freundlich: This empirical model can be applied to multilayer adsorption, with a non-homogeneous distribution of adsorption energies. The Freundlich model is criticized by the lack of thermodynamic consistency, and not behaving according to Henry's law at low gas concentrations. Moreover, this model does not provide an adsorption limit at high gas concentrations. The activation energy for desorption is estimated as $E_d = E_d^o exp(-\alpha\theta_{NH_3})$.

- Temkin: This model is the most common used for NH_3 adsorption over vanadium-based SCR catalysts. It considers an empirical parameter for the adsorbate-support interaction, α. The adsorption energy decreases linearly as the coverage increases due to the increase of interactions

with adjacent species. However, in a catalyst with low concentration of active sites, the interaction between adsorbed species is negligible. For the standard Temkin model, the desorption energy is estimated as $E_d = E_d^o(1 - \alpha\theta_{NH_3})$, while for the modified Temkin model, the desorption energy is estimated as $E_d = E_d^o.(1-\alpha\theta_{NH_3}^{\beta})$. Table 2.4 shows parameters for NH_3 adsorption in a vanadium-based SCR catalyst using a Temkin model [93].

	V_2O_5 / TiO_2	V_2O_5-WO_3 / TiO_2	Commercial
k_a^o (m^3/mol.s)	0.820	0.487	33.87
k_d^o (1/s)	3.67x10^6	2.67x10^5	2.20x10^6
E_d^o (kcal/mol)	25.8	22.9	23.0
α	0.310	0.405	0.256

Table 2.4: NH_3 adsorption Temkin model parameters for a vanadium-based SCR catalyst [34], [93].

- Empirical dual site coverage: This empirical model developed by Lietti et al. [93], provides a coverage dependence on the existence of two adsorption sites, with different adsorption energies. The desorption energy is estimated as $E_d = E_d^o + Btanh(-\alpha\theta_{NH_3} + A)$. This model provides better NH_3 adsorption estimations at low temperatures and during fast transients. However, the parameters do not have a physical meaning.

At equilibrium, the ratio between the adsorption and desorption rate constants is called the equilibrium constant K_c, which is defined in Eq. 2.2 where C_i is the gas concentration in (mol/m^3), and γi is the reaction order [91].

$$K_c = \prod_{i=1}^{n} C_i^{\gamma_i} \tag{2.2}$$

For ideal gases, the equilibrium constant K_c can be converted to the dimensionless thermodynamic equilibrium constant, K as shown in Eq. 2.3 [92].

$$\begin{aligned} K &= K_c\Big(\frac{RT}{P_{ref}}\Big)^{\delta} \\ \delta &= \sum \gamma_i \end{aligned} \tag{2.3}$$

This will allow to relate to the Gibbs free energy change, ΔG, between the

gas molecule and its adsorbed state as presented in Eq. 2.4.

$$RT\ln(K) = -\Delta G \tag{2.4}$$

The thermodynamic equilibrium constant, K, can be expressed in terms of the enthalpy change ΔH, and entropy change ΔS, as presented in Eq.2.5, since the Gibbs free energy change ΔG, is related to the enthalpy and entropy as shown in Eq. 2.6 [91].

$$K = exp\Big(\frac{-\Delta H_{ads} + T\Delta S_{ads}}{RT}\Big) \tag{2.5}$$

$$\Delta G = \Delta H - T\Delta S \tag{2.6}$$

In Eq. 2.5, ΔH_{ads} is the adsorption enthalpy change and ΔS_{ads} is the adsorption entropy change from the gas molecule to the adsorbed state over the catalyst surface. As a result, it is possible to define an NH_3 adsorption model for describing the adsorption isotherms [91]. The adsorption model is defined by thermodynamic parameters with physical meaning about the bonding strength between the gas molecules and the surface, and their spatial arrangement [91], [92]. Therefore, with the equilibrium state defined, just one phenomenon, adsorption or desorption, needs to be estimated for describing the adsorption/desorption steps completely, since the equilibrium characterization provides the way to relate the adsorption and desorption rates.

Parameter estimation approaches

For adsorption models, e.g. Langmuir, linear least squares methods are used for parameter estimation, which are solved in matrix form in a fast and efficient way. This involves a transformation, usually logarithmic, of the adsorption isotherm equation for the parameters to be linear. However, the obtained parameters can differ based on the transformation and method (more than 40% of the expected parameters' value), and the assumption on error variance normally distributed is violated [96], [97]. Therefore, the best approach for finding a proper adsorption model for inferences involves non-linear methods, which are based on iterative algorithms [78], [89].

The parameters are tuned based on an objective function, which is minimized or maximized to get the best representation from the experimental

data [98]. Different objective functions will lead to different parameters, and for non-linear parameter estimation, more than one function is recommended for evaluation and model discrimination. Variations are also identified on the estimated parameters [89]. Table 2.5 shows some of the error functions that can be minimized on parameter estimation [89], [94], [96].

Error function	**Nomenclature**	**Equation**
Least square sum	LSS	$LSS = \sum_{i=1}^{n} (y_{mod} - y_{exp})_i^2$
Sum of absolute errors	EABS	$EABS = \sum_{i=1}^{n} \lvert y_{mod} - y_{exp} \rvert_i$
Average relative error	ARE	$ARE = \frac{100}{n} \sum_{i=1}^{n} \left\lvert \frac{y_{mod} - y_{exp}}{y_{exp}} \right\rvert$
Marquardt's standard deviation	MSD	$MSD = \sqrt{\frac{1}{n-p} \sum_{i=1}^{n} \left[\frac{y_{exp} - y_{mod}}{y_{exp}} \right]^2}$

Table 2.5: Error function used as objective functions in parameter estimation

Any error function used for parameter estimation has two components: the pure error variance due to the measurement noise and the lack-of-fit due to the deficiencies in the model structure and estimated parameters [79]. The noise present in the data can be estimated by repeated measurements, and the lack-of-fit can be estimated with an F-test, which should give lower values than the noise estimate to be significant [88], [89].

Most of the error functions used for parameter estimation are based on the least square approach, where a set of parameters is found minimizing the sum of residuals. In the Maximum likelihood estimator (MLE), the aim is to maximize the probability function given the data, and assuming a model structure [78], [90]. Nevertheless, if the residual is assumed to be normally distributed and independent, the least squares and Maximum likelihood give

the same estimates [98].

A sequential fitting strategy is usually implemented to minimize correlation and make the optimization problem for parameter estimation easy to converge [78], [80]. A sequential strategy includes data segmentation and multiple initial estimates for getting closer to the global optimum. For preliminary fitting, the temperature dependency of some parameters can be removed, reducing the amount of parameters [88]. Then, using previous studies or heuristics, it is possible to use these parameters as initial estimates [92].

A cross-validation procedure is recommended at the end of the fitting strategy. In this procedure the model is evaluated under different datasets, by randomly dividing the experimental dataset [99]. Cross-validation increases the model robustness accounting for uncertainties in using a experimental dataset with limited size. For randomly dividing the dataset, the k-fold cross-validation method partitions the original dataset into k equally distributed subsets randomly (usually k=5) [100], [101]. Then one subset is used as the validation set while k-1 subsets are used as the modeling development set. The model parameters are estimated k times. Each time, one subset is assigned to the validation set while the remaining subsets, k-1, become the model development set. The final model parameters and performance are estimated as the mean value of the obtained parameters and performance during the k iterations [99], [101].

Model discrimination

An indicator criterion for model discrimination should include a balance between goodness of fit and parsimony. In other words, a model should achieve a level of generalization, being able to predict new data from the same phenomenon, while avoiding overfitting. Most of the objective functions used for parameter estimation, just focus on goodness of fit, while the parsimony is analyzed subjectively.

Currently, there are different indicators balancing goodness-of-fit and parsimony being used in model discrimination. The most common indicators are: the Akaike information criterion (AIC), the Bayesian Information criterion (BIC), and the adjusted predicted sum of squares (APRESS) presented in Table 2.6 [90], [98]. In Table 2.6, LSS refers to the Least Squared Sum value for the model, n is the sample size and p is the number of model parameters. These criteria have two terms: the first term measures the prediction error

and the second is a penalty for increasing parameters. The model with the lowest value of any of these indicators is selected as the best model [78].

Indicator name	Nomenclature	Equation
Akaike information Criterion	AIC	$AIC = n * log(LSS/n) + 2(p+1)$
Bayesian Information Criterion	BIC	$BIC = n * log(LSS/n) + (p+1) * log(n)$
Adjusted predicted sum of squares	APRESS	$APRESS = \left(\frac{1}{1-(p+1)\alpha/n}\right)^2 * (LSS/n)$

Table 2.6: Goodness-of-fit indicators for model discrimination [86], [90]

As noted in Table 2.6, the APRESS criterion needs the estimation of a tune parameter, α, which involves an iterative process for finding an optimal value where several parameters are computed simultaneously. In addition, this criterion is computing intensive since a two-step optimization is required: first to find the tuning factor, then to find the model parameters. On the other hand, BIC is used for descriptive statistics, providing a way to identify most relevant features. In the same way, AIC is recommended when prediction is the main goal, since it approximates the Kullback-Leiber information theory for models [90], [102]. Moreover, for complex models, as the data size grows, AIC is able to identify subtle effects in the model, increasing accuracy. Therefore, AIC is an appropriate criterion for model selection, since it focuses on replicability, getting the best approximation of reality, and providing quantitative understanding of the studied phenomenon [86], [98]. Nevertheless, a comprehensive modeling development process needs to be complemented by the evaluation of different indicators, increasing the model's confidence.

In general, the coefficient of determination, R^2 (Eq. 2.7), is recommended for descriptive statistics and should be extended to non-linear parameter estimation with caution. The R^2 compares the fit with the simplest possible model, an horizontal line with zero slope. However, it has been found that for non-linear models, it is possible to have R^2 values higher than one, which could be interpreted as a low quality fit with wide confidence interval in the

parameters [89]. Furthermore, it could be a negative number, that could explain that the model is performing worse than a horizontal line. The adjusted R^2 has the same drawbacks but it accounts for the relationship between the sample size and the degree of freedom [78], [89].

$$R^2 = 1 - \frac{\sum(y_{exp} - y_{mod})}{\sum(y_{exp} - \bar{y})} \tag{2.7}$$

Finally, for model discrimination, a quality assessment for ruling-out overfitting issues is usually performed. This involves the estimation of the pair-wise correlation matrix between parameters and the confidence interval estimation. The methods used for linear regression can be extended to the non-linear case, by estimating the Jacobian over a small perturbation (around 1%), where a linear behavior can be assumed [89].

The Akaike Information Criterion (AIC)

The Akaike Information Criterion (AIC) is based on the Kullback-Leibler information theory for model selection based on information losses. In the Kullback-Leibler information theory, reality is given for data but unknown to the modeler, so there is a distance between a true model, $f(x)$, and an approximate model with a set of parameters θ, $g(x|\theta)$, given by the Eq. 2.8 [78], [98].

$$I(f,g) = \int f(x)log(f(x))dx - \int f(x)log(g(x|\theta))dx \tag{2.8}$$

Eq. 2.8 measures the discrepancies expressed as the distance from $g(x|\theta)$ to $f(x)$, where the main objective in parameter estimation is to get the distance as close to $f(x)$. The true model, $f(x)$ is not possible to know, but the set of approximate models can be compared in relative terms since knowing $f(x)$ is not required as shown in Eq. 2.9 [78], [86]. However, this method provides a relative value which only has meaning when it is compared in a set of candidate models.

$$I(f,g) - \int f(x)log(f(x))dx = -\int f(x)log(g(x|\theta))dx \tag{2.9}$$

The AIC provides a way to calculate the relative distances, or expectations on getting closer to a true model, without knowing $f(x)$, and the maximum

likelihood estimator (MLE) for the estimated parameters, $\hat{\theta}$, which can be approximated as presented in Eq. 2.10 [86], [90].

$$AIC = -2log(MLE(\hat{\theta}(x))) + 2K \tag{2.10}$$

Where K is the bias correction term, penalizing the complexity of the model. If the residuals are assumed to be independent and normally distributed, the least squares and maximum likelihood theory have identical estimates. The AIC is a relative value which is compared to the different AIC values from the model candidates set with different complexity [78], [90]. The best model is the one with the lowest AIC value. However, the difference between the AIC values between models, ΔAIC_i, needs to be considered since smaller changes indicate that more than one model is relevant for representing the data [102]. The difference between the AIC values between models is calculated as Eq. 2.11.

$$\Delta AIC_i = AIC_i - AIC_{min} \tag{2.11}$$

The ΔAIC_i provides a ranking for the candidate models, which can be evaluated based on some heuristics described in Table 2.7 [78]. The best model has a ΔAIC value of zero. However, if there are other models with ΔAIC values around 0 to 10, more experimental data or modifications on the candidate model set are required to be able to select a single model from the model discrimination process [98].

ΔAIC_i change	Level of support by the data
0-2	Relevant
4-7	Partly relevant
7-10	Vaguely relevant
>10	Data does not support the model

Table 2.7: ΔAIC heuristics for model discrimination [78]

CHAPTER 3

Experimental

In the following section, a description of the experiment and pre-processing method for obtaining NH_3 adsorption isotherms over a vanadium-based SCR catalyst using a gas flow reactor is presented. The experiments involve a wide experimental region at different temperatures, NH_3 concentrations, water concentrations and catalyst oxidation states (oxidized and reduced). For obtaining the adsorption isotherms, a robust experimental method was developed, assuring steady-state conditions and repeatibility. Moreover, since time-series data is obtained from the different measurement devices in the gas flow reactor setup, a data processing method was developed to estimate the adsorption equilibrium base points for the adsorption isotherm. The development of the experimental method and the data-processing method was the objective of **Paper A**. The obtained experimental data help to obtain the appropriate information about the system for inference by modeling and complement other experimental methods such as the Temperature Programmed Desorption (TPD).

3.1 Gas flow reactor

A gas flow reactor is used for the NH_3 adsorption experiments. A scheme of the gas flow reactor is shown in Fig. 3.1. The setup can be divided in three sections: flow adjustment, reactor and gas analysis. In the flow adjustment section, the gas flow and composition are defined by the use of mass flow controllers (MFCs). In the current setup there are multiple MFCs with different operating ranges, since it is recommended to operate the MFC at a higher valve opening for higher accuracy. Therefore, before performing an experiment, a valve allocation optimization is required, assigning the most suitable MFCs for the experiment. In the reactor zone, the temperature is controlled and the monolith sample is placed. The reactor zone assures isothermal condition and stable flow. Last, the gas analysis zone, is where the outlet gas composition is measured by a Fourier transform infrared (FTIR) spectrometer. The main components of the gas flow reactor setup are listed in Table 3.1, with their purpose and used reference.

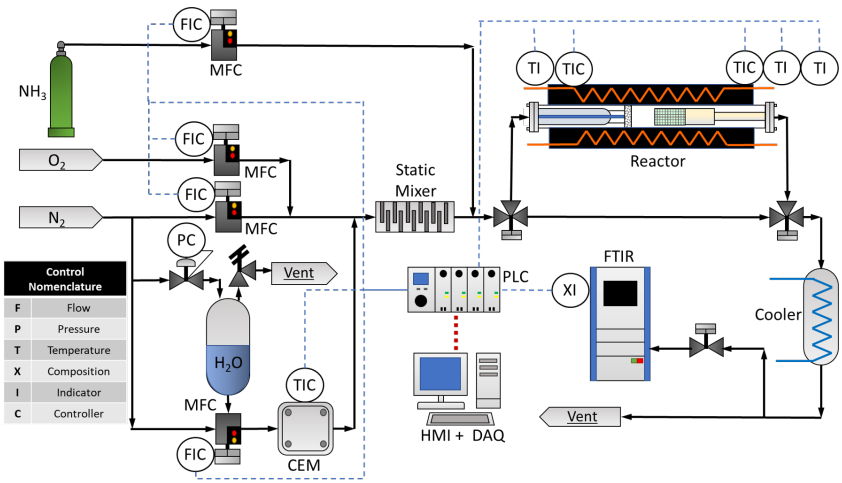

Figure 3.1: Experimental setup scheme

There are some considerations in the experimental setup for reliable measurements:

- All the piping is kept at 180°C to avoid water condensation and minimize

Table 3.1: Gas flow reactor main components

Component	Reference	Principle / Function
MFC (Mass Flow Controller)	Bronkhorst ® EL-FLOW Select	Flow is measured and controlled based on the thermal mass flow principle.
CEM (Controlled evaporator and mixer) module	Bronkhorst ®	Water and N_2 are mixed and heated to ensure water vapor flow.
Coriolis Flow Meter	Bronkhorst ® MINI-CORIFLOW-M13	Water flow is measured and controlled based on the Coriolis principle.
Thermocouples	Type K Class 1	Change of voltage due to thermoelectric effect.
FTIR gas analyzer	AVL Sesam i60 FT	Fourier transform infrared spectrometer, for measuring gas concentrations.
O_2 sensor	Magnos 106 O_2 sensor	Paramagnetic sensor.
HMI and DAQ	ProControl Dizanta Suite + MatLab	Human Machine Interface (HMI) for control and Data Adquisition system (DAQ) tool.

the gas adsorption over the pipes.

- Nitrogen is used as carrier gas.
- Two different NH_3 concentrations were used for operating the MFC at optimal conditions: a high concentration gas bottle of 3.6% and a low concentration bottle of 1.0%. This results in two experimental plans based on the NH_3 gas bottle concentration and the experimental region to track.
- Before an experiment, the FTIR spectrometer was calibrated with the built-in protocol.
- The setup was checked for leaks at each run.

The reactor zone in the setup has a special arrangement to ensure even flow distribution and isothermal conditions. The reactor is divided in two zones: the preheating zone is the larger zone, since the flow is heated to the specified temperature, and the reaction zone, where the sample is placed and the temperature sensors are located to measure temperature profiles over the sample. Each region has its own temperature control, integrated into a cascade control. The reactor zone arrangement is presented in Fig 3.2.

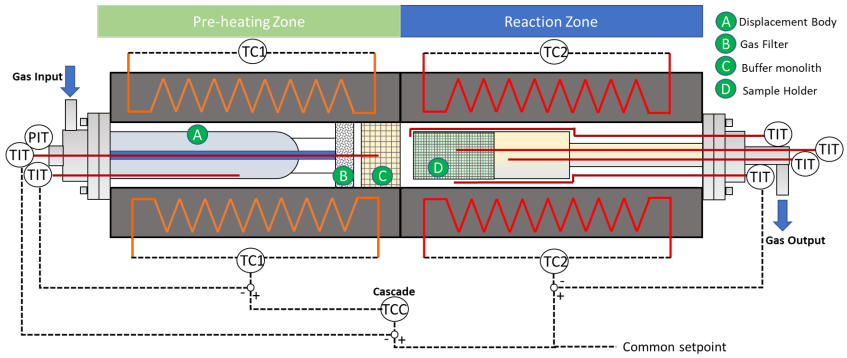

Figure 3.2: Reactor configuration. The dashed line represents the cascade control scheme between the two reactor zones, where TIT is a temperature transmitter and TC is a temperature control element.

3.2 Experiment for Adsorption isotherms

NH_3 adsorption experiments were performed for a state-of-the-art vanadium-based SCR catalyst supplied by Umicore. It is a washcoated monolith with TiO_2 as support and tungsten (W) as promoter. Two different washcoat loadings with the same formulation were supplied. They were used to obtain independent observations and increase the dataset size. Moreover, lower NH_3 concentrations were achieved with a low concentration bottle (1.0%). In these tests a small volume - low loading sample was used. The three samples are described in Table 3.2.

Table 3.2: Main catalyst sample parameters

ID	Type	Length (cm)	Diameter (cm)	Weight (g)	Nominal Washcoat Loading (g/L)
HC-LL	High concentration, low loading	7.64	2.43	20.67	288
HC-HL	High concentration, high loading	7.68	2.48	23.77	371
LC-LL	Low concentration, low loading	2.66	2.52	7.15	288

Before using the samples in the experiments, a degreening protocol was

run to stabilize the catalyst and remove adsorbates from the catalytic surface. The protocol is explained in Table 3.3. The stabilization was established when two consecutive SCR activity measurements were constant. Then, before an adsorption sequence at a specific temperature, a pretreatment protocol was performed for setting the catalyst state. Two states were defined: oxidized state obtained with O_2 oxidation and reduced state obtained with subsequent NH_3 reduction. The pretreatment is described in Table 3.4.

Table 3.3: Sample degreening steps for the catalyst samples

Procedure	**Step**	**Flow (NL/min)**	**Temp. (C)**	**Composition**	**Time (min)**
De-greening	Purging	30	450	5% H_2O	5
	SCR Activity	30	450	500ppm NO, 500ppm NH_3, 5% H_2O	5
	Stabilizing	30	450	5% H_2O, 5% O_2	10, 20, 60
	Final Purging	30	450	N_2 only	5
	Oxidizing	30	450	5% O_2	20

Table 3.4: Sample pre-treatment steps for defining catalyst oxidation state

Catalyst State	**Step**	**Flow (NL/min)**	**Temp. (C)**	**Composition**	**Time (min)**
Oxidized State	Purging	50	500	N_2 only	3
	Oxidizing	50	500	5% O_2	10
	Purging	50	500	N_2 only	3
Reduced State	Purging	50	500	N_2 only	3
	Oxidizing	50	500	5% O_2	10
	Purging	50	500	N_2 only	3
	Reduction	50	500	500ppm NH_3	20
	Purging	50	500	N_2 only	3

After the pretreatment, the temperature and water concentration were set to the NH_3 adsorption experiment conditions. The experiment is presented and described in Fig 3.3. It initiates with a high concentration step: 1000 ppm for the high concentration experiment and 150 ppm for the low concentration experiment. The first adsorption step is not required to reach equilibrium, since the adsorption estimation is done by integrating the difference between

the inlet and outlet NH_3 concentrations. Thus, different steady-state desorption steps define the adsorption isotherm. The sequence goes from high concentration to low concentration. This procedure was chosen since the desorption steps reach equilibrium faster as removing excess is a faster process than the opposite. The desorption step sequence was repeated twice for each experiment to get replicate data and for the flow calibration step in the data processing method described later. Isotherms were obtained at different water concentrations: 0, 0.5 and 5%, and the NH_3 gas concentration was set between 30 to 75 ppm for the low concentration experiments and between 75 to 450 ppm for the high concentration experiments. The total gas flow was set to 50 NL/min. For the oxidized catalyst the temperature range for the experiment was from 100 to 250°C since at higher temperatures NH_3 oxidation cannot be neglected. For the reduced catalyst the temperature range was from 100 to 400°C, at higher temperature NH_3 adsorption was not observed.

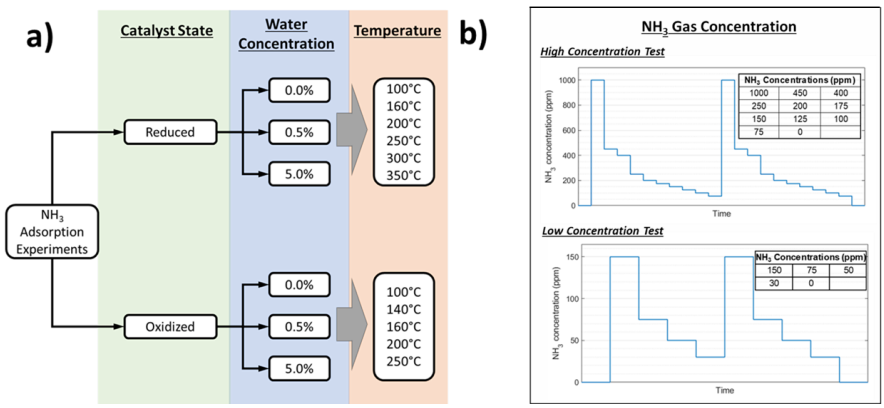

Figure 3.3: NH_3 adsorption experiments, (a) Conditions for the catalyst state, water concentration, and temperature, and (b) NH_3 concentration steps sequence for high concentration and low concentration experiments.

3.3 Data processing for modeling

From each experiment, there are two signals used for the estimation of the NH_3 adsorption isotherm but they need to be processed first, according to the proposed data processing method explained in this project. The signals are:

NH_3 gas flow rate obtained from the MFC at the reactor inlet, q_{MFC}, and NH_3 mole fraction at the outlet from the FTIR analyzer, y_{FTIR}. The processing method aims to calculate the accumulation over the catalyst obtained as:

$$n_{\mathrm{NH_3}} = F_{total} \int_0^{t_{int}} (y_{inert} - y_{FTIR})\, dt \tag{3.1}$$

Where F_{total} is the total gas molar flow, t_{int} is the duration of each desorption step, and y_{inert} is the concentration at the reactor outlet for an inert tracer gas with no interaction with the setup, which if obtained from the input signal q_{MFC}, and the Residence Time Distribution (RTD) model of the reactor following the preprocessing method presented in Fig 3.4.

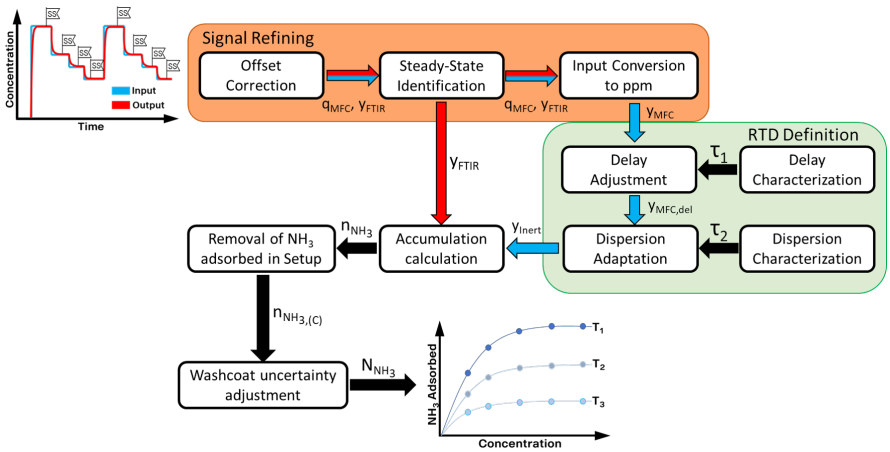

Figure 3.4: Data processing proposed method for estimating NH_3 adsorption isotherms

Each step in the proposed data processing method is explained below:

- **Signal refining:** In this step, the offset from the FTIR signal, y_{FTIR}, the identification of the steady-state at each desorption step using a statistical criterion, and the conversion of the input flow signal, q_{MFC}, to concentration, y_{MFC}, are determined by using reference values from the FTIR analyzer.
- **RTD definition:** The input concentration signal, y_{MFC} is shifted in time by delay and dispersion effects presented in a real reactor and

characterized by a RTD model. Therefore, the input signal will resemble a signal obtained from an inert tracer at the outlet, y_{inert}. The RTD was characterized by an independent set of experiments in the gas flow reactor to parametrize the delay and dispersion time constant at different flows, temperatures, MFC locations and FTIR measurements.

- **Accumulation calculation:** With the processed signal, accumulated NH_3 over the catalyst is estimated with eq. 3.1, for each desorption step.
- **Removal of NH_3 adsorbed in setup:** A correction was implemented since NH_3 was found to be adsorbed over the experimental setup, overestimating the adsorption value over the catalyst. A Langmuir two-site adsorption model was developed to account for the NH_3 adsorbed on the experimental setup at different temperatures, water concentrations and NH_3 concentrations.
- **Washcoat uncertainty adjustment:** For increasing the sample size, all the adsorption values were normalized by the washcoat loading to be comparable. However, some deviations were observed and a continuous and smooth adsorption isotherm is still preferable. Therefore, an optimization algorithm was developed to adjust the washcoat loading, within 10% of the nominal value, to account for the production uncertainties and the washcoat distribution deviations observed in the sample when inspected.

CHAPTER 4

Modeling

The data-driven modeling framework proposed for developing an NH_3 adsorption model for a vanadium-based SCR catalyst is presented in the following section and explained in **Paper B**. The proposed modeling framework includes different steps for building feasible adsorption model candidates based on proposed adsorption mechanisms aimed to capture the features from the NH_3 adsorption isotherm data obtained in **Paper A**. Several adsorption models were evaluated and their parameters were estimated by a three-step parameter estimation workflow using different objective functions with increased complexity at each step. Then, a reconciliation step is proposed for integrating the best models from the different parameter estimation workflows into a single unified adsorption model with an optimal set of parameters. However, for a robust model, not affected by the dataset nature, a cross-validation step is proposed. The obtained NH_3 adsorption model from the overall modeling workflow, was derived from the intensive evaluation of multiple model candidates and the different steps towards an optimal and robust set of parameters maximizing the amount of information from the data described by the model. Furthermore, a quality assessment was performed to increase the model's validity and the model parameters were related to earlier studies at molecular

scale.

The modeling framework is illustrated in Fig. 4.1 which shows two different workflows for parameter estimation based on segmenting the data into two subsets: oxidized and reduced. The segmentation of data benefits the parameter estimation process since opposite conditions such as oxidized/reduced or wet/dry could create conflicts on finding the global minima in the objective function used for parameter estimation.

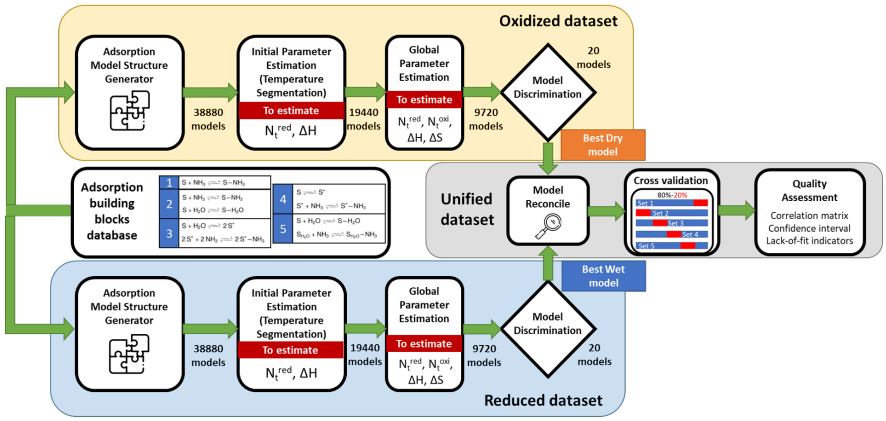

Figure 4.1: Data-driven modeling framework for evaluation and discrimination of NH_3 adsorption models.

4.1 Adsorption Model formulation

Multiple NH_3 adsorption sites with different dynamics have been identified for vanadium-based SCR catalysts from previous studies. Therefore, an NH_3 adsorption model must be able to capture this diversity and its effects on the NH_3 storage capacity. According to this, an adsorption model assumes different types of adsorption sites where NH_3 adsorbs. As a result the total amount of NH_3 adsorbed over the catalyst is the sum of the NH_3 adsorbed at the different sites assumed in the catalyst as presented in Eq. 4.1.

$$q_{\mathrm{NH_3}} = \sum_{j=1}^{M} N_j \theta_j \tag{4.1}$$

Table 4.1: Site specific adsorption mechanisms forming the building blocks of the adsorption model.

Mechanism			Coverage
A	Simple adsorption	$S + NH_3 \rightleftarrows S-NH_3$	$\theta = \frac{K_c C_{NH_3}}{1+K_c C_{NH_3}}$
B	Site activation	$S \rightleftarrows S^*$ $S^* + NH_3 \rightleftarrows S^*-NH_3$	$\theta = \frac{K_{c1} K_{c2} C_{NH_3}}{1+K_{c1}+K_{c2} C_{NH_3}}$
C	Competitive adsorption	$S + NH_3 \rightleftarrows S-NH_3$ $S + H_2O \rightleftarrows S-H_2O$	$\theta = \frac{K_{c1} C_{NH_3}}{1+K_{c2} C_{H_2O}+K_{c1} C_{NH_3}}$
D	Water activated adsorption	$S + H_2O \rightleftarrows S^*$ $S^* + NH_3 \rightleftarrows S^*-NH_3$	$\theta = \frac{K_{c1} K_{c2} C_{NH_3} C_{H_2O}}{1+K_{c1} C_{H_2O}+K_{c1} K_{c2} C_{NH_3} C_{H_2O}}$
E	Site duplication by water	$S + H_2O \rightleftarrows 2\,S^*$ $2\,S^* + 2\,NH_3 \rightleftarrows 2\,S^*-NH_3$	$\theta = \frac{K_{c1} K_{c2} C_{NH_3} C_{H_2O}}{1+2K_{c1} C_{H_2O}+2K_{c1} K_{c2} C_{NH_3} C_{H_2O}}$

Where q_{NH_3} is the total NH_3 adsorption capacity in mol NH_3/g$_{washcoat}$, N_j is the total amount of sites of type j in mol/g$_{washcoat}$ and θ_j is the NH_3 coverage of site j. The NH_3 coverage of a site j, θ_j, is determined by assigning an adsorption mechanism from a defined set capturing the main features from the NH_3 adsorption isotherm dataset. Each type is assigned an adsorption mechanism, which is derived assuming a Langmuir adsorption model. The proposed mechanisms are presented in Table 4.1 and explained below:

- Simple adsorption: In this mechanism only NH_3 adsorbs on the site.
- Site activation: The adsorption site is activated before adsorbing NH_3. The activation is temperature-dependent.
- Competitive adsorption: NH_3 and water compete for adsorption sites which results in decreased NH_3 storage capacity.
- Water activated adsorption: In this mechanism, water activates a site

for NH_3 adsorption.

- Site duplication by water: In this mechanism the site is activated and duplicated by water. Then, NH_3 can adsorb on the site.

At equilibrium, the coverage for each adsorption mechanism can be expressed in terms of the equilibrium constant, K_c, which is converted to the dimensionless thermodynamic equilibrium constant, K, related to the Gibbs free energy, ΔG, and hence the adsorption enthalpy, ΔH_{ads}, and the adsorption entropy, ΔS_{ads} as presented in Eq. 4.2.

$$K = exp\Big(\frac{-\Delta H_{ads} + T\Delta S_{ads}}{RT}\Big) \tag{4.2}$$

The adsorption enthalpy, ΔH_{ads}, and the adsorption entropy, ΔS_{ads}, are parameters to be predicted by the parameter estimation workflow. For reducing the number of parameters, the adsorption entropy, ΔS is specified as a global parameter applying to all the adsorption site types assumed in the catalyst. Four different values can be designated to the adsorption entropy based on the adsorption nature: ΔS_1 for adsorbed NH_3, ΔS_2 for adsorbed water, ΔS_3 for site activation, and ΔS_4 for site duplication.

Moreover, for the number of adsorption sites of type j, a parameter is considered for the oxidized catalyst, N_j^{oxi}, and another for the reduced catalyst, N_j^{red}.

4.2 Model structure generator

A systematic procedure for generating a feasible set of model candidates was developed by the combination between the assumed number of adsorption site types and the adsorption mechanisms. As a result, a large set of model candidates is generated, combining the adsorption mechanisms (r=5) and assuming the catalyst could contain up to six types of adsorption sites (M=1,..,6). There are 461 possible models obtained from the combination arrangement presented in Eq. 4.3.

$$C_{M,r} = \binom{M+r-1}{r-1} = \frac{(M+r-1)!}{(M-1)!r!} \tag{4.3}$$

Fig. 4.2 shows the possible model structures generated by this method,

which assign a specific set of parameters based on the adsorption mechanisms and number of adsorption site types.

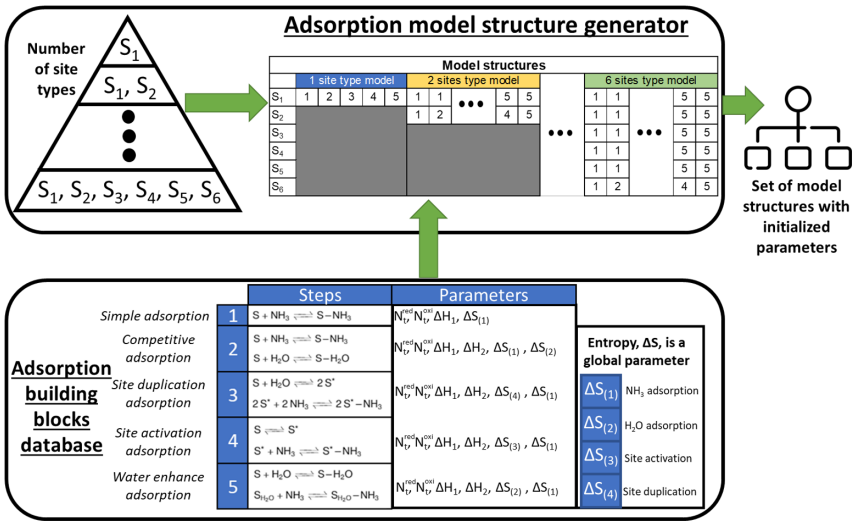

Figure 4.2: Adsorption model structure generator.

4.3 Parameter estimation workflow

The parameter estimation workflow involves three steps using different objective functions, with increased complexity at each step. This allows a robust evolution towards the global minimum in a highly non-linear problem. For the NH_3 adsorption model development, two different workflows are performed by segmenting the dataset. One workflow was assigned to the oxidized dataset, and another to the reduced dataset. Furthermore, at each step in the parameter estimation workflow, 50% of the best models are chosen to continue to the next step.

The first step in the parameter estimation workflow is intended for parameter initialization, by defining initial estimates for the parameters and different allocation of the dataset within the adsorption site types assumed in the catalyst. As a result of this multiple initialization, around 33,000 scenarios were specified for evaluation in the first step by using the Least square sum (LSS)

objective function presented in Eq. 4.4.

$$LSS = \sum_{i=1}^{n} (q_{mod} - q_{exp})_i^2 \tag{4.4}$$

In the second step, over 18,000 scenarios for parameter estimation were computed by using the Marquardt's objective function to minimize, see Eq. 4.5. This objective function has the advantage to normalize the residual and include a penalty on model complexity defined by the number of parameters, p, in the model.

$$MSD = \frac{1}{n-p} \sum_{i=1}^{n} \left[\frac{q_{exp} - q_{mod}}{q_{exp}} \right]^2 \tag{4.5}$$

The third step is a parameter fine tuning for around 9,000 scenarios selected from the previous step by using a custom-made objective function named Slope tracking presented in Eq. 4.6.

$$MST = \frac{1}{n-p} \left[\lambda \sum_{i=1}^{n} \frac{\left[q_{exp} - q_{mod})\right]^2}{q_{exp}^2} + (1-\lambda) \sum_{j=1}^{m} \frac{\left[\alpha_{exp} - \alpha_{mod})\right]^2}{\alpha_{exp}^2} \right] + ln \left[\lambda \sum_{i=1}^{n} \frac{\left[q_{exp} - q_{mod})\right]^2}{q_{exp}^2} - (1-\lambda) \sum_{j=1}^{m} \frac{\left[\alpha_{exp} - \alpha_{mod})\right]^2}{\alpha_{exp}^2} \right]^2 \tag{4.6}$$

This custom-made objective function includes a slope comparison between the experimental slope, α_{exp} and the model slope, α_{mod}, at three different locations at each isotherm. The slope is calculated as the gradient between the NH_3 storage capacity and the NH_3 gas concentration as shown in Eq. 4.7.

$$\alpha = \frac{\Delta q}{\Delta C}\Big|_T \tag{4.7}$$

Furthermore, the Slope tracking function includes a new parameter, λ, which balances the contribution between the residual and the slope's comparison by including a penalty term.

4.4 Model discrimination and reconciliation

For each parameter estimation workflow, using the oxidized and reduced dataset, the 20 best models were chosen for a more detailed model discrimination process. Choosing a small set of model candidates helps on the visualization of the results from this step. First, the model performance was estimated by calculating the Akaike Information Criteria, presented in Eq. 4.8.

$$AIC = n * log\left(\frac{1}{n}\sum_{i=1}^{n}\left[\frac{q_{exp} - q_{mod}}{q_{exp}}\right]^2\right) + 2(p+1) \tag{4.8}$$

This criterium evaluates the maximum likelihood estimator as an indicator of fitting performance and it adds a penalty on model complexity. Then, an overfitting evaluation is done by the estimation of the pair-wise correlation between parameters using the method from linear models which can be extended to non-linear models if the Jacobian is estimated over a small perturbation.

The best model for the oxidized workflow and the best one for the reduced workflow are chosen as the ones with the lowest AIC value and lowest correlation distribution. They are used in the reconciliation step where a unified model is built by separating the similarities into a common set of parameters and the differences in specific set of parameters for the oxidized and reduced dataset. For the reconciliation step, the parameters in the unified model are estimated by using the Slope tracking objective function. This results in a unified NH_3 adsorption model with an optimal set of parameters with physical interpretation.

4.5 Robust models by cross-validation

The optimal set of parameters obtained for the unified model, is influenced by the dataset used in the parameter estimation. As a result, it is possible to obtain another set of optimal parameters if the dataset was different. A robust model is not influenced by the used dataset and it is expected to perform satisfactory under different datasets. Therefore, in this step a robust set of parameters is determined by using a k-fold cross-validation method.

In this method, shown in Fig. 4.3, the full dataset is divided randomly into k subsets equally distributed (k=5 in this study). Then, the parameters are estimated k times, by assigning one subset as the validation set and k-1

subsets as the ones used for parameter estimation.

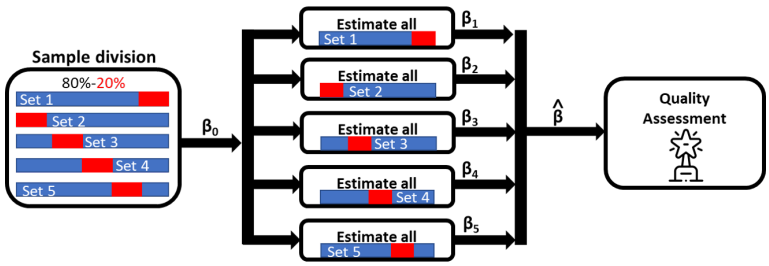

Figure 4.3: k-fold cross-validation for robust modeling.

The robust set of parameters is obtained by calculating the mean value from all the k parameter sets. This robust set of parameters accounts to the uncertainties of the dataset. Afterwards, a quality assessment for the unified model with the robust set of parameters is performed. It involves the estimation of different lack-of-fit indicators and the correlation matrix between parameters. For improvement on the design of the experiment, a local residual analysis is performed, identifying the region that could benefit from additional experiments.

CHAPTER 5

Results and Discussion

A summary of the main results from the proposed experimental and data pre-processing method for obtaining NH_3 adsorption isotherms for a vanadium-based SCR catalyst using a gas flow reactor is presented in this section. The results include NH_3 adsorption isotherms over a wide experimental region, with increased resolution and repeatability. The pre-processing method with its steps is discussed, revealing the importance of the Residence Time Distribution (RTD) model for real reactor characterization and the identification and quantification of systematic artifacts which can be removed from the data. A detailed description of the proposed experimental and pre-processing method, and implications on the enhanced adsorption data for modeling purposes is provided in **Paper A**.

Furthermore, this section includes the results from the modeling framework developed in **Paper B**, to obtain an NH_3 adsorption model that captures the main features of the NH_3 adsorption isotherms obtained in **Paper A**. A multi-site Langmuir adsorption model framework was implemented by the definition of multiple model structures combining pre-defined adsorption mechanisms with the number of site types assumed in the catalyst. In a data-driven modeling framework, the best model is selected by the evaluation and

discrimination of several models using lack-of-fit and parameter correlation indicators. These allow the determination of the best model for describing the NH_3 adsorption isotherms for a vanadium-based SCR catalyst. Finally, the obtained parameters are related to previous computational and experimental studies increasing their validity.

5.1 Experimental

The proposed data processing method aimed for the estimation of NH_3 adsorption capacity for a vanadium-based SCR catalyst. This was achieved by gas flow reactor characterization with a Residence Time Distribution (RTD) model and the removal of artifacts. Three different samples on washcoat loading and volume were used for this study and they were normalized by the washcoat loading for making the dataset comparable and to extend the sample size. However, a smooth and continuous isotherm is required for modeling purposes and an additional step for adjusting the washcoat loading due to manufacturing deviations was included. The adjusted washcoat loading for all the samples deviates less than 10% from the nominal value. The advantages of the proposed method are illustrated in Fig. 5.1, where the same isotherm is presented without (panel a) and with (panel b) the data processing method. On panel A, the three different samples cannot produce a smooth isotherm, and repeated measurements with the same sample are spread. The benefits of the method, illustrated in panel b, are the following: the resolution of the adsorption isotherm is increased since the data dispersion is reduced, and the overestimation from the artifacts is removed. Therefore a continuous, smooth and increasing adsorption isotherm is obtained.

The NH_3 adsorption isotherms obtained with the proposed experimental and data processing method over the wide experimental region of different temperatures, NH_3 gas concentrations, water gas concentrations and catalyst states are presented in Fig 5.2.

Different aspects on NH_3 adsorption over the vanadium-based SCR catalyst were identified. The adsorption isotherms reach values closer to saturation (plateau) at low NH_3 concentration and there is a small increase in adsorption capacity when the NH_3 gas concentration is increased. Moreover, the figure shows how the adsorption capacity decreases with temperature. The saturation level (plateau) is reached at different NH_3 storage capacities at different

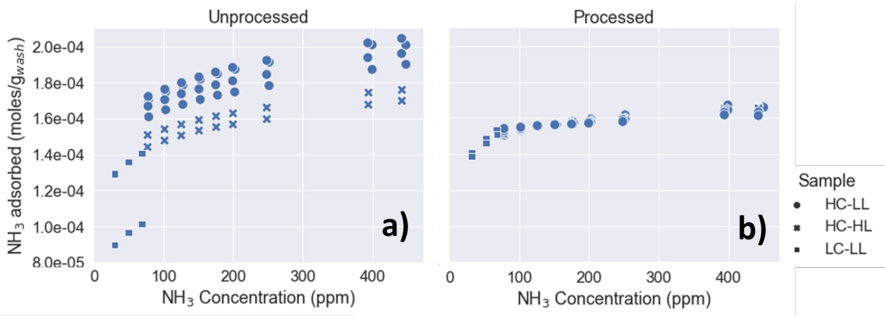

Figure 5.1: NH_3 adsorption isotherm at 100°C, for the oxidized catalyst sample at 0.5% water concentration based on (a) unprocessed data and (b) processed data.

temperatures reflecting the complexity of the catalyst surface where multiple adsorption sites are present. This has been observed in other earlier studies at molecular scale with experiments and DFT calculations. Furthermore, the NH_3 adsorption behavior shows to be different from the oxidized and reduced catalyst. For the oxidized catalyst the adsorption capacity is higher, and water promotes the NH_3 storage capacity at low concentrations (0.5%) due to the creation of new Brønsted sites. However, at high concentrations (5.0%), water decreases the NH_3 adsorption, which can be attributed to competitive adsorption. For the reduced catalyst, water has an inhibitory effect in all studied concentrations as a result of competitive adsorption with NH_3. The reduced catalyst can be re-oxidized in a reversible process where the catalyst is restored at its fully oxidized condition. The above explains the importance of the re-oxidation step in the SCR mechanism since the reaction cannot move forward if NH_3 does not adsorb. However, for the reduced catalyst, NH_3 can still adsorb, indicating the diversity of adsorption sites, where some sites are more prone to be reduced by NH_3 in the pretreatment step than others.

The obtained adsorption isotherms provide detailed information for modeling purposes, involving several adsorption sites over the catalyst surface, the nature change between reduced and oxidized catalyst state, the water influence on the NH_3 adsorption capacity, and the activation of sites due to temperature for reaching different adsorption saturation levels. From the results presented in Fig. 5.2 the model has to capture the water effect, which involves competitive adsorption in the reduced catalyst and in the oxidized catalyst at high

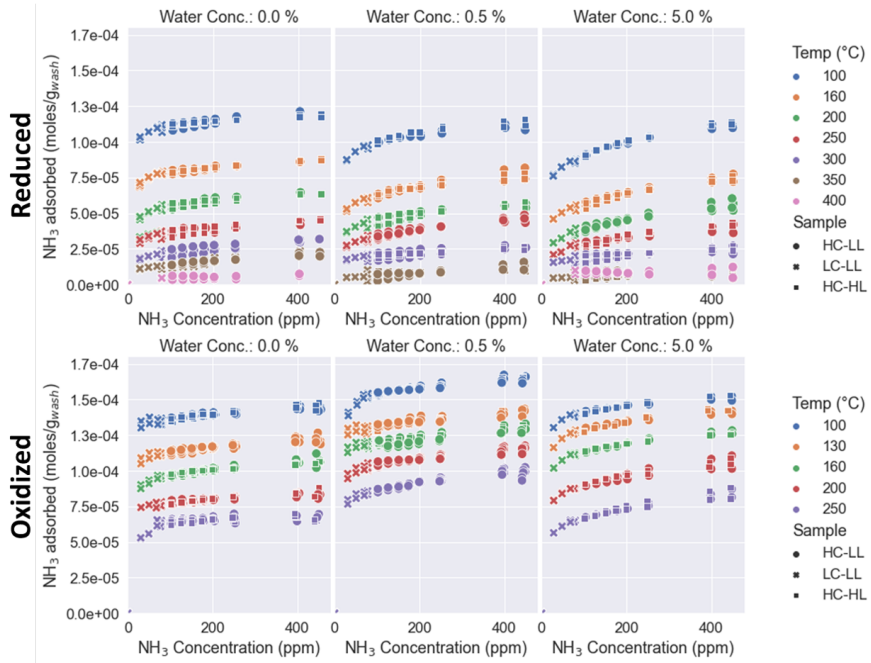

Figure 5.2: Adsorption isotherms for NH_3 on a vanadium-based SCR catalyst for different oxidation states of the catalyst and different water concentrations.

water concentration (5.0%). On the other hand, water increases the NH_3 adsorption capacity in the oxidized sample at low water concentration (0.5%), which can be explained by the creation of new Brønsted acidic sites. With the NH_3 adsorption isotherm data obtained with the proposed experimental and pre-processing method in **Paper A**, the definition of a suitable adsorption model for the NH_3 adsorption over a vanadium-based SCR catalyst was the main scope of the **Paper B**.

Experimental method assessment

The proposed method provides systematic steps for obtaining data with high resolution, low dispersion, and well-defined regions for proper inference. This can be observed on the effect of water concentration on the NH_3 adsorption

for the oxidized catalyst as shown in Fig, 5.3. Fig. 5.3 presents the average adsorption capacity for an NH_3 gas concentration between 125 ppm and 400 ppm for the unprocessed and processed data. In the unprocessed data, it is not possible to identify the subtle effect on water at low water concentration since the high dispersion gives no statistical significance. On the other side, the processed data provides a well defined range with low dispersion, adequate for inferences about the observed phenomena.

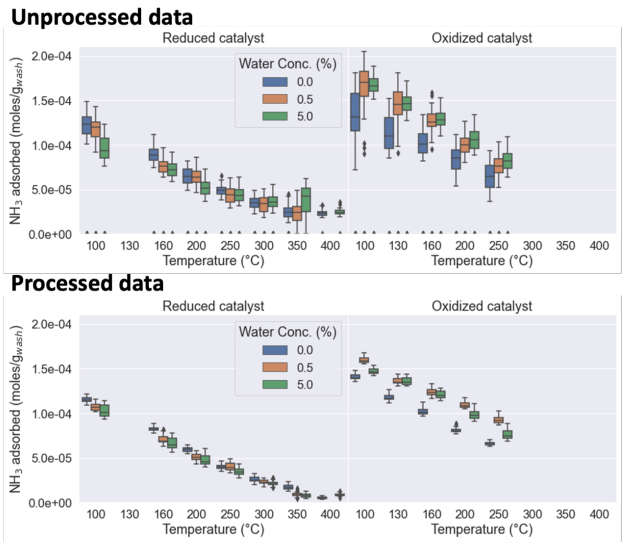

Figure 5.3: Average adsorption capacity for NH_3 concentrations in the range 125 to 400 ppm for different water concentrations, temperatures and catalyst oxidation states.

Another advantage of the proposed method is the possibility to identify and quantify the contribution of each data processing step in the reduction of the NH_3 adsorption capacity overestimation. Fig. 5.4 presents the results of this analysis for the reduced and oxidized catalyst. Some steps, such as the RTD characterization and the NH_3 adsorbed in the experimental setup, provide similar values between catalyst states since they depend on the experimental setup. However, their relative contribution on the NH_3 adsorption value is higher for the reduced catalyst since the NH_3 adsorption over the catalyst is lower and the artifacts have a higher effect on the estimated value.

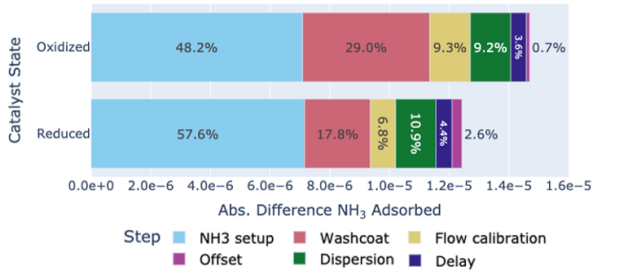

Figure 5.4: Contribution of each preprocessing step in the overestimation magnitude between unprocessed and processed data.

As a result, this method offers a new alternative in the analysis of different phenomena from experiments performed in a gas flow reactor under transient conditions, such as reaction and regeneration, with low dispersion, high repeatability and a systematic approach.

5.2 Modeling

A 5-site NH_3 adsorption model was selected from the data-driven modeling process developed in **Paper B**. The model structure and obtained parameters are outlined in Table 5.1. The model involves a single site with an NH_3 simple adsorption mechanism, three sites with a competitive adsorption mechanism and a single site with a water activated adsorption mechanism.

Table 5.1: Selected NH_3 adsorption model mechanism structure and parameters with confidence interval.

	S_j-N^{red} (mol/g_{wash})	S_j-N^{oxi} (mol/g_{wash})		Mechanism	ΔH_{ads} (kJ/mol)	ΔS_{ads} (J/mol.K)
Site 1	3.26E-05 +/- 6.86E-07	2.92E-05 +/- 5.94E-07	A	$S + NH_3 \rightleftharpoons S-NH_3$	-109.91 +/- 7.6	-173.58 +/- 2.8
Site 2	2.03E-05 +/- 5.10E-07	4.85E-05 +/- 1.05E-06	C	$S + NH_3 \rightleftharpoons S-NH_3$	-155.25 +/- 1.2	-173.58 +/- 2.8
				$S + H_2O \rightleftharpoons S-H_2O$	-91.73 +/- 1.2	-100.59 +/- 1.7
Site 3	2.90E-05 +/- 5.54E-07	2.58E-05 +/- 1.08E-06	C	$S + NH_3 \rightleftharpoons S-NH_3$	-127.98 +/- 9.4	-173.58 +/- 2.8
				$S + H_2O \rightleftharpoons S-H_2O$	-130.08 +/- 4.9	-100.59 +/- 1.7
Site 4	4.29E-05 +/- 8.20E-07	4.18E-05 +/- 5.94E-07	C	$S + NH_3 \rightleftharpoons S-NH_3$	-95.56 +/- 6.3	-173.58 +/- 2.8
				$S + H_2O \rightleftharpoons S-H_2O$	-49.03 +/- 1.0	-100.59 +/- 1.7
Site 5	1.89E-05 +/- 4.46E-07	4.80E-05 +/- 1.05E-06	D	$S + H_2O \rightleftharpoons S-H_2O$	-60.96 +/- 2.3	-100.59 +/- 1.7
				$S_{H_2O} + NH_3 \rightleftharpoons S_{H_2O}-NH_3$	-153.56 +/- 6.4	-173.58 +/- 2.8

The model captures the main features from the experimental data as showed in Fig. 5.5. These features are: the different saturation levels at different temperatures and the NH_3 storage reduction for the reduced catalyst compared with the oxidized catalyst. In addition, water dynamics reduce the NH_3 storage capacity in the reduced catalyst and also in the oxidized catalyst at high water concentrations (5.0%). On the other hand, water increases the NH_3 storage capacity at low water concentrations (0.5%).

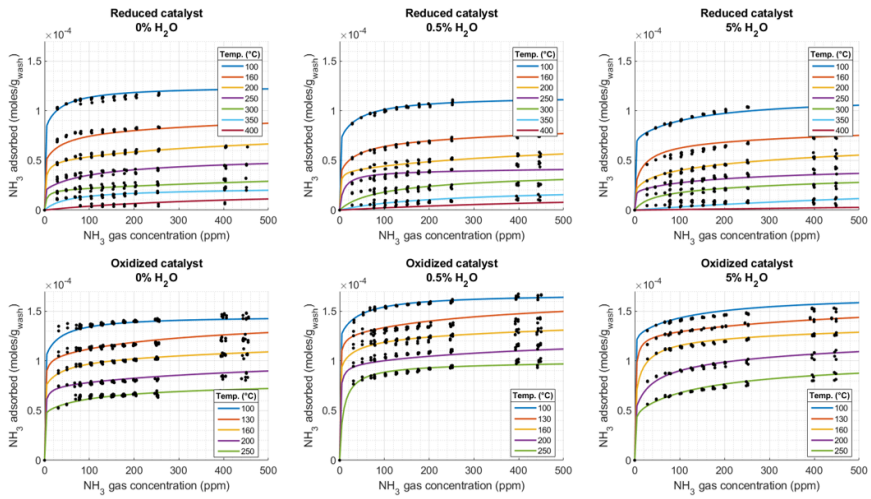

Figure 5.5: NH_3 adsorption model fitting performance for the experimental adsorption isotherms. Model values (continuous line) and experimental data (black circles).

The relevance of the sites is evaluated from the values in Table 5.1 and summarized in Fig. 5.6. For the reduced catalyst, the two most important sites have a competitive adsorption and a simple adsorption mechanism (site 4 and 1), while for the oxidized catalyst, the two most important sites involve a water activated adsorption and a competitive adsorption mechanism (site 2 and 5). Furthermore, some sites are not affected by the catalyst state, as seen in sites 1,2 and 4.

The adsorption enthalpies, ΔH_{ads}, are also reported in Table 5.1 and compared with corresponding values obtained from DFT studies in Fig. 5.7. The NH_3 adsorption enthalpy varies from -155 to -95 kJ/mol, and the water

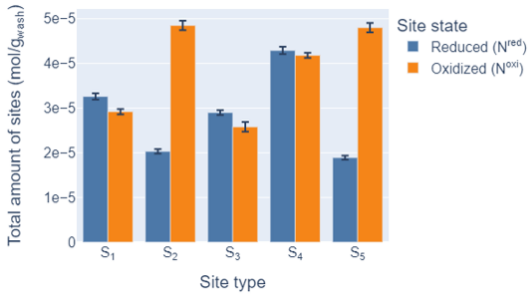

Figure 5.6: Total number of sites for each site type for the reduced catalyst, N^{red}, and the oxidized catalyst, N^{oxi}.

adsorption enthalpy ranges from −130 to −49 kJ/mol. For water, enthalpy values are lower than for NH_3 which is in line with previous studies. Furthermore, for site 3 the adsorption enthalpies for NH_3 and water have similar values, −127 and −130 kJ/mol, respectively. The enthalpies obtained for the NH_3 adsorption model are within the range of values reported for vanadium and titanium oxide clusters obtained in DFT studies.

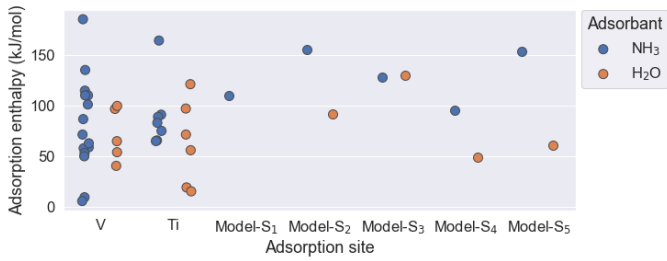

Figure 5.7: Adsorption enthalpy, ΔH_{ads}, comparison between DFT studies for vanadium and titanium clusters, and the model values.

The adsorption entropy, ΔS_{ads}, is defined as two global variables outlined in Table 5.1. ΔS_1 with a value of −173 J/mol·K for NH_3, and ΔS_2 with a value of −100 J/mol·K for water. From these values, the NH_3 adsorption is highly localized, with the NH_3 molecule losing most of its degrees of freedom while for water adsorption, the water molecule keeps some mobility over the catalytic surface being relevant for activating sites for NH_3 adsorption.

The 95% confidence interval was also evaluated for checking overfitting issues and presented in Fig. 5.8. The parameters with the widest confidence intervals are the adsorption enthalpies, ΔH, for sites 1, 3 and 4, with a range of 7% the original value. Nevertheless, these parameters are significant and these results do not suggest overfitting issues.

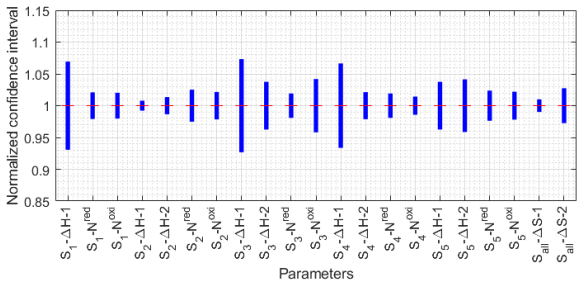

Figure 5.8: 95% normalized confidence interval for the model parameters

Finally, the correlation matrix was calculated for analyzing the parameter pair-wise interaction and presented in Fig. 5.9. High correlation values should be analyzed to neglect overfitting issues but for the NH_3 adsorption model, high correlation values are expected since it is a highly non-linear model and the adsorbed species the adsorption sites interact with each other on the catalyst surface. The detailed analysis of the correlation matrix is presented in **Paper B**, which shows the potential of this matrix to make inferences about the adsorption behavior and interaction between sites.

Data-driven modeling process discussion

The data-driven modeling process proposed in **Paper B** involves the evaluation of a large candidate model set generated systematically. The parameter estimation was performed in three steps where around 33,000, 18,000 and 9,000 estimation assignments were evaluated respectively. Fig. 5.10 shows the fitting performance at each step for each parameter estimation assignment and the evolution towards better fitting performance achieved by the use of different objective functions with increased complexity.

Then, for a detailed model discrimination, the 20 best models for the oxidized and reduced workflow were chosen and the fitting performance was

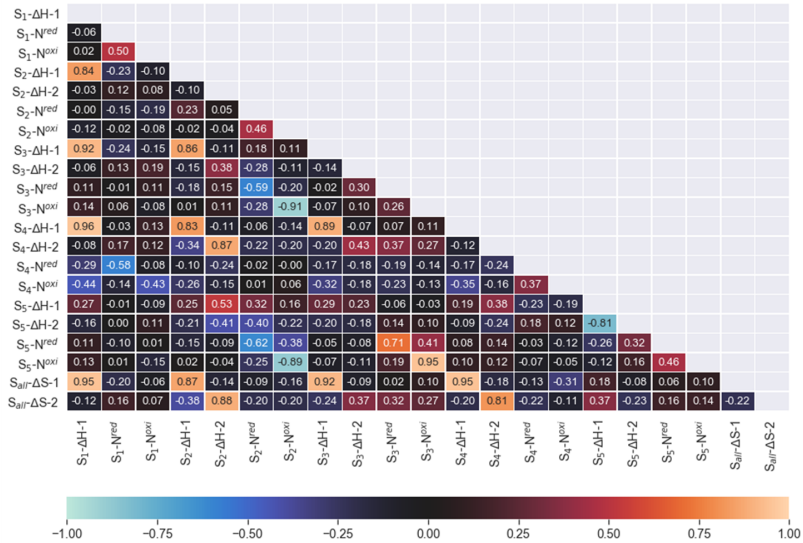

Figure 5.9: Correlation matrix for the selected NH_3 adsorption model.

evaluated and reported in Table 5.2. In the table, different indicators were used and gave similar results. In addition, the best models have fewer parameters than the rest, supporting the balance between high performance and low model complexity achieved in the modeling process.

The correlation matrix was calculated for each model, and summarized in a correlation distribution presented for all the models in Fig. 5.11. The best models have the lowest correlation between parameters and few outliers due to the non-linear nature of the NH_3 adsorption model. For the reduced model, model 1 exhibits the lowest correlation distribution and the best fitting performance as outlined in Table 5.2. However, for the oxidized model, model 1 does not have the lowest correlation distribution but it is close and fitting performance is the main indicator for model selection.

The model reconciliation step consisted on finding similarities between the best model for the reduced and oxidized workflow to build one unified model. For the two models, similar site mechanisms were prioritized followed by similar values on the adsorption enthalpy. As a result, it was found that the two models share a simple adsorption mechanism site with similar adsorption

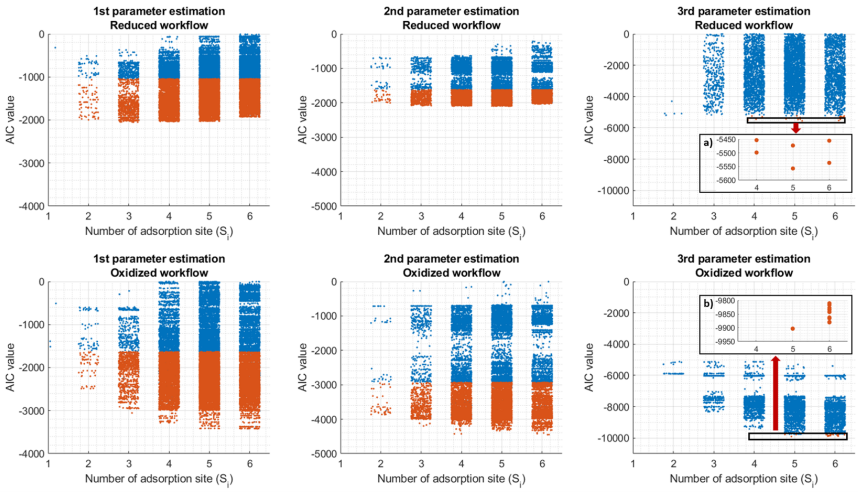

Figure 5.10: Fitting performance at different parameter estimation steps, evaluated by the AIC indicator. Orange points are the solutions used in the next step. Panel a) and b) are the magnified view around the best model region.

Table 5.2: Fitting performance summary for the 20 best models in the oxidized and reduced workflow.

Reduced workflow						Oxidized workflow					
Model ID	Mechanism	p	LSS	AIC	Marquardt	Model ID	Mechanism	p	LSS	AIC	Marquardt
1	ACAAC	20	50.52	-5557.07	0.239	1	AACCD	20	0.56	-9903.22	0.194
2	BACCAC	25	50.79	-5536.37	0.242	2	BCCCD	23	0.57	-9880.21	0.196
3	BDCB	19	52.25	-5498.59	0.246	3	ABCDCC	26	0.57	-9879.20	0.201
4	CCAEB	23	52.53	-5472.81	0.250	4	CCCEAA	25	0.58	-9865.17	0.199
5	BCCCBB	27	52.60	-5455.19	0.246	5	CCCEBB	28	0.57	-9862.41	0.198
6	BDCA	18	53.56	-5453.08	0.248	6	CCDCA	21	0.58	-9842.40	0.202
7	ABCBA	21	53.64	-5440.07	0.249	7	CBCCAD	26	0.59	-9841.81	0.200
8	BBCDC	23	53.58	-5432.46	0.336	8	CCBDC	23	0.59	-9833.96	0.203
9	BDCDC	23	55.06	-5376.95	0.319	9	CCCDAE	26	0.59	-9827.71	0.201
10	AACECC	25	55.80	-5344.84	0.245	10	CECACA	25	0.60	-9816.43	0.201
11	BCCDC	23	56.11	-5338.54	0.285	11	CCCADB	26	0.60	-9810.65	0.203
12	AACECB	26	56.27	-5322.81	0.244	12	CBCDC	23	0.60	-9797.98	0.203
13	BDCCBE	28	56.35	-5309.95	0.254	13	CCCAD	21	0.61	-9797.23	0.199
14	ABCDAC	25	57.05	-5300.11	0.253	14	BDDCCC	27	0.61	-9790.50	0.201
15	BCCDBD	27	56.82	-5298.04	0.267	15	ACCBEC	27	0.61	-9783.93	0.207
16	ABCC	18	57.90	-5295.02	0.257	16	CCCEAB	27	0.61	-9783.58	0.209
17	ABCABE	26	58.12	-5257.02	0.254	17	CCCAEA	25	0.62	-9775.96	0.238
18	BECCDE	28	58.19	-5244.75	0.387	18	CCCEBA	27	0.62	-9773.55	0.237
19	BDCCBE	19	59.22	-5244.05	0.262	19	CCEBC	24	0.62	-9761.34	0.236
20	ABCAD	21	59.27	-5237.24	0.438	20	CBCCE	24	0.62	-9759.58	0.249

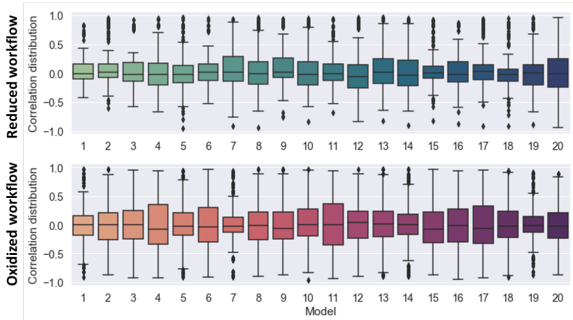

Figure 5.11: Pair-wise parameter correlation distribution for the 20 best models in the oxidized and reduced workflow.

enthalpies. Also, three sites with a simple or competitive adsorption of NH_3 mechanisms in the models were reconciled based on similar enthalpy values. For these three sites, simple adsorption mechanisms were changed to competitive adsorption mechanism since they capture the interactions with water. Finally, a competitive adsorption mechanism site has the same enthalpy as a water activated adsorption mechanism site. Here, the water activated adsorption mechanism was chosen since it is the only mechanism in the unified model that describes the increase of the NH_3 storage capacity in presence of water.

For the unified adsorption model, a cross-validation step was performed for obtaining robust parameters that account for data uncertainties. The results are presented in Fig. 5.12. The new parameter values changed less than 0.5 standard deviations, which do not change the physical significance.

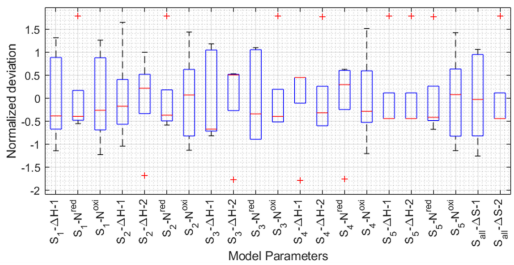

Figure 5.12: Cross-validation results for the selected NH_3 adsorption model. The red line represents the mean value used as the final value for the unified robust model.

CHAPTER 6

Concluding Remarks and Future Work

This thesis is aimed to develop a systematic, reliable and accurate method from improving the model fitting performance for catalysts used in the emission after-treatment system. The methods developed in this study were applied on finding the best NH_3 adsorption model for describing the equilibrium state in a state-of-the-art vanadium-based SCR catalyst. This was achieved by developing an experimental and pre-processing method for obtaining artifact-free experimental data with high resolution using a gas flow reactor, which is the most versatile experimental setup for kinetic studies used in the industry and academia. The developed method involved the reactor characterization by a residence time distribution (RTD) model for estimating the delay and dispersion times in the experimental setup, and the identification and quantification of artifacts.

Then, a data-driven processing process was developed to find the best mechanistic NH_3 adsorption model within the framework of Langmuir adsorption models. In the data-driven process, the purpose was to find the best model describing the experimental data from a massive set of model candidates. A 5-site adsorption model was chosen as the best model for describing the wide experimental region that considers different temperatures, NH_3 concen-

trations, water concentrations and catalyst state. The 5-site model involves mechanisms such a simple adsorption, competitive adsorption where water competes for adsorption sites, and water activated adsorption where water activates and adsorption site for NH_3 adsorption. The obtained robust model shows superior fitting performance over a wide experimental region with satisfactory quality assessment results. Furthermore, it was possible to relate the obtained values for the parameters with physical significance about the different adsorption sites on the catalyst surface and the interaction between adsorbates on these sites. For instance, the model reveals that NH_3 has a higher adsorption enthalpy than water since NH_3 is a stronger base than water. However for one site with a competitive adsorption mechanism, the desorption enthalpies for NH_3 and water are similar which suggest an adsorption site in the support which is not a Brønsted or Lewis acidic site.

Additionally, the model suggests that three adsorption sites are not affected by the catalyst state, since the NH_3 storage capacity remains stable between the oxidized and reduced state. Moreover, the adsorption entropy from the model, indicates a highly localized adsorption for NH_3 while for water, some mobility over the surface is feasible, which explains the water dissociation for site activation in the catalyst.

In this thesis we propose a new data-driven modeling process for kinetic models, which is not limited to the parameter estimation step performed in most of kinetic studies. The method is based the formulation of multiple feasible models, that are complex quantitative hypothesis, and evaluated with different initialization states to avoid local minima. Therefore, the maximization of usable information from the experimental data let us choose the best model based on fitting performance. The use of a large set of candidate models, reduces the probability of neglecting the best models for evaluation. However, it involves the implementation of computational methods to handle the multiple optimization assignments. Furthermore, the search for the global optima for the models, was performed by developing a sequential and robust parameter estimation workflow, where different objective functions with higher complexity benefit convergence and fitting performance.

6.1 Outlook

Even though the obtained model just describes the NH_3 adsorption behavior at equilibrium, it provides relevant information and parameters for achieving a transient NH_3 adsorption model with increased fitting performance, and high validity since satisfactory prediction at steady-state conditions is a requirement for a proper transient kinetic model. Therefore, the obtained results from this study will be used for the model development process for the transient NH_3 adsorption model.

Moreover, the NH_3 adsorption model gives interesting results on the difference between the oxidized and reduced catalyst, which will be investigated for characterizing the different adsorption sites and their interaction and their potential role as active sites in the SCR mechanism. As a result, a set of reaction steps between number of sites in the reduced catalyst, $S_i - N^{red}$, and the number of sites in the oxidized $S_i - N^{oxi}$ could be achieved.

Furthermore, the experimental and modeling framework developed in this study could be used for studying the NH_3 adsorption phenomena in the vanadium-based SCR catalyst after a controlled aging protocol, since the effect of aging on the NH_3 storage capacity is relevant for the industrial application. Additionally, this method could be validated by obtaining an NH_3 adsorption model for a copper-functionalized zeolite SCR catalyst, where higher NH_3 storage capacities are expected but further studies are required to investigate the water dynamics and the role of oxygen.

Finally, the computational methods developed in this study are already deployed in a high-performance computer cluster but they can be optimized for faster computation and better resource utilisation. This will involve the improvement of the current methods, including new variables for the proper configuration of the computing cluster.

References

[1] G. H. Brundtland, "Our common future—call for action," *Environmental Conservation*, vol. 14, no. 4, pp. 291–294, 1987.

[2] W. V. Reid, *Millennium ecosystem assessment*. 2005.

[3] K. Popper, *Conjectures and refutations: The growth of scientific knowledge*. routledge, 2014.

[4] J. Teter, P. Cazzola, T. Gul, E. Mulholland, P. Le Feuvre, S. Bennett, P. Hugues, Z. Lagarde, V. Kraayvanger, T. Bryant, *et al.*, "The future of trucks: Implications for energy and the environment," 2017.

[5] IEA. (2019). "World energy outlook 2019," [Online]. Available: `https://www.iea.org/reports/world-energy-outlook-2019` (visited on 09/01/2012).

[6] BP, *BP energy outlook 2019*, 2020.

[7] Y. Kaya, M. Yamaguchi, and O. Geden, "Towards net zero CO_2 emissions without relying on massive carbon dioxide removal," *Sustainability Science*, vol. 14, no. 6, pp. 1739–1743, 2019.

[8] U.S. EIA. (2020). "Use of energy explained: Energy use for transportation," [Online]. Available: `https://www.eia.gov/energyexplained/use-of-energy/transportation-in-depth.php` (visited on 09/01/2012).

[9] S. Gross, "The challenge of decarbonizing heavy transport," 2020.

[10] OECD, "Energy and air pollution: World energy outlook special report 2016," 2016.

[11] I. Manisalidis, E. Stavropoulou, A. Stavropoulos, and E. Bezirtzoglou, "Environmental and health impacts of air pollution: A review," *Frontiers in public health*, vol. 8, p. 14, 2020.

[12] CARB. (2017). "Zero emission vehicle (ZEV) program," [Online]. Available: https://ww2.arb.ca.gov/our-work/programs/zero-emission-vehicle-program (visited on 09/01/2012).

[13] W. F. Lamb, T. Wiedmann, J. Pongratz, R. Andrew, M. Crippa, J. G. Olivier, D. Wiedenhofer, G. Mattioli, A. Al Khourdajie, J. House, *et al.*, "A review of trends and drivers of greenhouse gas emissions by sector from 1990 to 2018," *Environmental Research Letters*, 2021.

[14] B. Plumer and N. Popovich. (2020). "Emissions are surging back as countries and states reopen," [Online]. Available: https://www.nytimes.com/interactive/2020/06/17/climate/virus-emissions-reopening.html (visited on 09/01/2012).

[15] ICCT. (2018). "Transportpolicy.net," [Online]. Available: https://www.transportpolicy.net/?title=Main_Page (visited on 09/01/2021).

[16] F. Rodriguez and F. Posada, "Future heavy-duty emission standards," *International Council for Clean Transportation*, 2019.

[17] ACEA. (2020). "ACEA position paper views on proposals for Euro 7 emission standard," [Online]. Available: https://www.acea.auto/files/ACEA_Position_Paper-Views_on_proposals_for_Euro_7_emission_standard.pdf (visited on 09/01/2021).

[18] EPA/NHTSA, "Final rule for greenhouse gas emissions and fuel efficiency standards for medium- and heavy-duty engines and vehicles - phase 2," 2016. [Online]. Available: https://www.epa.gov/regulations-emissions-vehicles-and-engines/final-rule-phase-2-greenhouse-gas-emissions-standards.

[19] ICCT. (2021). "ICCTs comments and technical recommendations on future Euro 7/VII emission standards," [Online]. Available: https://theicct.org/sites/default/files/eu-commission-euro-7-and-VI-may2021.pdf (visited on 09/01/2021).

[20] TE. (2020). "Road to zero: The last EU emission standard for cars, vans, buses and trucks," [Online]. Available: https://www.transportenvironment.org/wp-content/uploads/2021/06/2020_04_Road_to_Zero_last_EU_emission_standard_cars_vans_buses_trucks.pdf (visited on 09/01/2021).

[21] D. Sperling and J. S. Cannon, *Reducing climate impacts in the transportation sector*. Springer, 2009.

[22] AGVES. (2020). "Preliminary findings on possible Euro 7 emission limits for LD and HD vehicles," [Online]. Available: https://circabc.europa.eu/sd/a/fdd70a2d-b50a-4d0b-a92a-e64d41d0e947/CLOVE%5C%20test%5C%20limits%5C%20AGVES%5C%202020-10-27%5C%20final%5C%20vs2.pdf (visited on 09/01/2021).

[23] Ö. Andersson and P. Börjesson, "The greenhouse gas emissions of an electrified vehicle combined with renewable fuels: Life cycle assessment and policy implications," *Applied Energy*, vol. 289, p. 116 621, 2021.

[24] G. Kalghatgi, "Is it really the end of internal combustion engines and petroleum in transport?" *Applied energy*, vol. 225, pp. 965–974, 2018.

[25] C. Sharp, G. Neely, B. Zavala, and S. Rao, "CARB low NO_X Stage 3 program-final results and summary," SAE Technical Paper, Tech. Rep., 2021.

[26] B. Zavala, C. Sharp, G. Neely, and S. Rao, "CARB low NO_X stage 3 Program-Aftertreatment evaluation and final demonstration system results," *SAE Technical Paper*, pp. 01–1402, 2020.

[27] S. Rao, J. Sarlashkar, S. Rengarajan, C. Sharp, and G. Neely, "A controls overview on achieving ultra-low NO_X," SAE Technical Paper, Tech. Rep., 2020.

[28] R. M. Heck, R. J. Farrauto, and S. T. Gulati, *Catalytic air pollution control: commercial technology*. John Wiley & Sons, 2016.

[29] I. Nova and E. Tronconi, *Urea-SCR technology for deNOx after treatment of diesel exhausts*. Springer, 2014, vol. 5.

[30] P. Lakshminarayanan and A. K. Agarwal, *Design and Development of Heavy Duty Diesel Engines: A Handbook*. Springer Nature, 2019.

[31] I. Chorkendorff and J. W. Niemantsverdriet, *Concepts of modern catalysis and kinetics*. John Wiley & Sons, 2017.

[32] K. Reif, *Diesel engine management*. Springer, 2014.

[33] M. Colombo, I. Nova, and E. Tronconi, "Detailed kinetic modeling of the NH_3–NO/NO_2 SCR reactions over a commercial Cu-zeolite catalyst for diesel exhausts after treatment," *Catalysis Today*, vol. 197, no. 1, pp. 243–255, 2012.

[34] I. Nova, C. Ciardelli, E. Tronconi, D. Chatterjee, and B. Bandl-Konrad, "NH_3-SCR of NO over a V-based catalyst: Low-t redox kinetics with NH_3 inhibition," *AIChE Journal*, vol. 52, no. 9, pp. 3222–3233, 2006.

[35] I. Nova, L. Lietti, E. Tronconi, and P. Forzatti, "Transient response method applied to the kinetic analysis of the $DeNO_X$–SCR reaction," *Chemical Engineering Science*, vol. 56, no. 4, pp. 1229–1237, 2001.

[36] E. Tronconi, I. Nova, C. Ciardelli, D. Chatterjee, B. Bandl-Konrad, and T. Burkhardt, "Modelling of an SCR catalytic converter for diesel exhaust after treatment: Dynamic effects at low temperature," *Catalysis Today*, vol. 105, no. 3-4, pp. 529–536, 2005.

[37] G. Ramis, G. Busca, F. Bregani, and P. Forzatti, "Fourier transform-infrared study of the adsorption and coadsorption of nitric oxide, nitrogen dioxide and ammonia on vanadia-titania and mechanism of selective catalytic reduction," *Applied Catalysis*, vol. 64, pp. 259–278, 1990.

[38] I. E. Wachs and B. M. Weckhuysen, "Structure and reactivity of surface vanadium oxide species on oxide supports," *Applied Catalysis A: General*, vol. 157, no. 1-2, pp. 67–90, 1997.

[39] N.-Y. Topsøe, M. Anstrom, and J. Dumesic, "Raman, FTIR and theoretical evidence for dynamic structural rearrangements of vanadia/titania $DeNO_X$ catalysts," *Catalysis letters*, vol. 76, no. 1, pp. 11–20, 2001.

[40] I. E. Wachs, G. Deo, B. M. Weckhuysen, A. Andreini, M. A. Vuurman, M. de Boer, and M. D. Amiridis, "Selective catalytic reduction of NO with NH_3 over supported vanadia catalysts," *Journal of Catalysis*, vol. 161, no. 1, pp. 211–221, 1996.

[41] J. Haber, A. Kozlowska, and R. Kozłowski, "The structure and redox properties of vanadium oxide surface compounds," *Journal of Catalysis*, vol. 102, no. 1, pp. 52–63, 1986.

[42] A. Åberg, A. Widd, J. Abildskov, and J. K. Huusom, "Parameter estimation and analysis of an automotive heavy-duty SCR catalyst model," *Chemical Engineering Science*, vol. 161, pp. 167–177, 2017.

[43] N. R. Jaegers, J.-K. Lai, Y. He, E. Walter, D. A. Dixon, M. Vasiliu, Y. Chen, C. Wang, M. Y. Hu, K. T. Mueller, *et al.*, "Mechanism by which tungsten oxide promotes the activity of supported V_2O_5/TiO_2 catalysts for NO_X abatement: Structural effects revealed by 51V MAS NMR spectroscopy," *Angewandte Chemie*, vol. 131, no. 36, pp. 12 739–12 746, 2019.

[44] N. Topsoe, H. Topsoe, and J. Dumesic, "Vanadia/titania catalysts for selective catalytic reduction (SCR) of nitric-oxide by ammonia: I. Combined temperature-programmed in-situ FTIR and on-line mass-spectroscopy studies," *Journal of Catalysis*, vol. 151, no. 1, pp. 226–240, 1995.

[45] F. J. Janssen, F. M. Van den Kerkhof, H. Bosch, and J. R. Ross, "Mechanism of the reaction of nitric oxide, ammonia, and oxygen over vanadia catalysts. 2. Isotopic transient studies with oxygen-18 and nitrogen-15," *Journal of Physical Chemistry*, vol. 91, no. 27, pp. 6633–6638, 1987.

[46] C. H. Bartholomew, "Mechanisms of catalyst deactivation," *Applied Catalysis A: General*, vol. 212, no. 1-2, pp. 17–60, 2001.

[47] J. A. Moulijn, A. Van Diepen, and F. Kapteijn, "Catalyst deactivation: Is it predictable?: What to do?" *Applied Catalysis A: General*, vol. 212, no. 1-2, pp. 3–16, 2001.

[48] Y. Liu, Z. Liu, B. Mnichowicz, A. V. Harinath, H. Li, and B. Bahrami, "Chemical deactivation of commercial vanadium SCR catalysts in diesel emission control application," *Chemical Engineering Journal*, vol. 287, pp. 680–690, 2016.

[49] H. Kamata, K. Takahashi, and C. I. Odenbrand, "Surface acid property and its relation to SCR activity of phosphorus added to commercial v_2o_5 (wo_3)/tio_2 catalyst," *Catalysis Letters*, vol. 53, no. 1-2, pp. 65–71, 1998.

[50] M. Turco, L. Lisi, R. Pirone, and P. Ciambelli, "Effect of water on the kinetics of nitric oxide reduction over a high-surface-area V_2O_5/TiO_2 catalyst," *Applied Catalysis B: Environmental*, vol. 3, no. 2-3, pp. 133–149, 1994.

[51] G. Busca, L. Lietti, G. Ramis, and F. Berti, "Chemical and mechanistic aspects of the selective catalytic reduction of NO_X by ammonia over oxide catalysts: A review," *Applied Catalysis B: Environmental*, vol. 18, no. 1-2, pp. 1–36, 1998.

[52] W. Wong and K. Nobe, "Kinetics of nitric oxide reduction with ammonia on" chemical mixed" and impregnated vanadium (V) oxide-titanium (IV) oxide catalysts," *Industrial & engineering chemistry product research and development*, vol. 23, no. 4, pp. 564–568, 1984.

[53] T. Komatsu, M. Nunokawa, I. S. Moon, T. Takahara, S. Namba, and T. Yashima, "Kinetic studies of reduction of nitric oxide with ammonia on Cu^{2+}-exchanged zeolites," *Journal of Catalysis*, vol. 148, no. 2, pp. 427–437, 1994.

[54] H.-G. Lintz and T. Turek, "Intrinsic kinetics of nitric oxide reduction by ammonia on a vanadia-titania catalyst," *Applied Catalysis A: General*, vol. 85, no. 1, pp. 13–25, 1992.

[55] S. Xiong, X. Xiao, Y. Liao, H. Dang, W. Shan, and S. Yang, "Global kinetic study of NO reduction by NH_3 over V_2O_5–WO_3/TiO_2: Relationship between the SCR performance and the key factors," *Industrial & Engineering Chemistry Research*, vol. 54, no. 44, pp. 11 011–11 023, 2015.

[56] N.-Y. Topsøe, "Mechanism of the selective catalytic reduction of nitric oxide by ammonia elucidated by in situ on-line fourier transform infrared spectroscopy," *Science*, vol. 265, no. 5176, pp. 1217–1219, 1994.

[57] M. Takagi, T. Kawai, M. Soma, T. Onishi, and K. Tamaru, "The mechanism of the reaction between NO_X and NH_3 on V_2O_5 in the presence of oxygen," *Journal of Catalysis*, vol. 50, no. 3, pp. 441–446, 1977.

[58] L. Arnarson, H. Falsig, S. B. Rasmussen, J. V. Lauritsen, and P. G. Moses, "A complete reaction mechanism for standard and fast selective catalytic reduction of nitrogen oxides on low coverage VO_X/TiO_2 (001) catalysts," *Journal of catalysis*, vol. 346, pp. 188–197, 2017.

[59] L. Arnarson L., H. Falsig, S. B. Rasmussen, J. V. Lauritsen, and P. G. Moses, "The reaction mechanism for the SCR process on monomer V^{5+} sites and the effect of modified Brønsted acidity," *Physical Chemistry Chemical Physics*, vol. 18, no. 25, pp. 17 071–17 080, 2016.

[60] G. He, Z. Lian, Y. Yu, Y. Yang, K. Liu, X. Shi, Z. Yan, W. Shan, and H. He, "Polymeric vanadyl species determine the low-temperature activity of V-based catalysts for the SCR of NO_X with NH_3," *Science advances*, vol. 4, no. 11, eaau4637, 2018.

[61] S. Soyer, A. Uzun, S. Senkan, and I. Onal, "A quantum chemical study of nitric oxide reduction by ammonia (SCR reaction) on V_2O_5 catalyst surface," *Catalysis today*, vol. 118, no. 3-4, pp. 268–278, 2006.

[62] C. Ciardelli, I. Nova, E. Tronconi, D. Chatterjee, T. Burkhardt, and M. Weibel, "NH_3 SCR of NO_X for diesel exhausts aftertreatment: Role of NO_2 in catalytic mechanism, unsteady kinetics and monolith converter modelling," *Chemical Engineering Science*, vol. 62, no. 18-20, pp. 5001–5006, 2007.

[63] J. Dumesic, N.-Y. Topsøe, H. Topsøe, Y. Chen, and T. Slabiak, "Kinetics of selective catalytic reduction of nitric oxide by ammonia over vanadia/titania," *Journal of catalysis*, vol. 163, no. 2, pp. 409–417, 1996.

[64] M. Zhu, J.-K. Lai, U. Tumuluri, Z. Wu, and I. E. Wachs, "Nature of active sites and surface intermediates during SCR of NO with NH_3 by supported V_2O_5–WO_3/TiO_2 catalysts," *Journal of the American Chemical Society*, vol. 139, no. 44, pp. 15 624–15 627, 2017.

[65] R.-M. Yuan, G. Fu, X. Xu, and H.-L. Wan, "Brønsted-NH^{4+} mechanism versus nitrite mechanism: New insight into the selective catalytic reduction of NO by NH_3," *Physical Chemistry Chemical Physics*, vol. 13, no. 2, pp. 453–460, 2011.

[66] X. Yin, H. Han, and A. Miyamoto, "Active site and mechanism of the selective catalytic reduction of NO by NH_3 over V_2O_5: A periodic first-principles study," *Physical Chemistry Chemical Physics*, vol. 2, no. 18, pp. 4243–4248, 2000.

[67] A. Vittadini, M. Casarin, and A. Selloni, "First principles studies of vanadia- titania monolayer catalysts: Mechanisms of NO selective reduction," *The Journal of Physical Chemistry B*, vol. 109, no. 5, pp. 1652–1655, 2005.

[68] Z. Zhao, E. Li, Y. Qin, X. Liu, Y. Zou, H. Wu, and T. Zhu, "Density functional theory (DFT) studies of vanadium-titanium based selective catalytic reduction (SCR) catalysts," *Journal of Environmental Sciences*, vol. 90, pp. 119–137, 2020.

[69] I. Song, H. Lee, S. W. Jeon, T. Kim, and D. H. Kim, "Time-resolved observation of V_2O_5/TiO_2 in NH_3-SCR reveals the equivalence of Brønsted and Lewis acid sites," *Chemical Communications*, vol. 56, no. 98, pp. 15 450–15 453, 2020.

[70] F. Giraud, C. Geantet, N. Guilhaume, S. Gros, L. Porcheron, M. Kanniche, and D. Bianchi, "Experimental microkinetic approach of De-NO_X by NH_3 on $V_2O_5/WO_3/TiO_2$ catalysts. 1. Individual heats of adsorption of adsorbed NH_3 species on a sulfate-free TiO_2 support using adsorption isobars," *The Journal of Physical Chemistry C*, vol. 118, no. 29, pp. 15 664–15 676, 2014.

[71] M. Anstrom, J. Dumesic, and N.-Y. Topsøe, "Theoretical insight into the nature of ammonia adsorption on vanadia-based catalysts for SCR reaction," *Catalysis letters*, vol. 78, no. 1, pp. 281–289, 2002.

[72] M. Anstrom, N.-Y. Topsøe, and J. Dumesic, "Density functional theory studies of mechanistic aspects of the SCR reaction on vanadium oxide catalysts," *Journal of Catalysis*, vol. 213, no. 2, pp. 115–125, 2003.

[73] V. Ranea, J. Vicente, E. Mola, P. Arnal, H. Thomas, and L. Gambaro, "Adsorption of H_2O on the (001) plane of V_2O_5: Chemisorption site identification," *Surface Science*, vol. 463, no. 2, pp. 115–124, 2000.

[74] P. Hejduk, M. Szaleniec, and M. Witko, "Molecular and dissociative adsorption of water at low-index V_2O_5 surfaces: DFT studies using cluster surface models," *Journal of Molecular Catalysis A: Chemical*, vol. 325, no. 1-2, pp. 98–104, 2010.

[75] H. S. Wahab, T. Bredow, and S. M. Aliwi, "Computational investigation of water and oxygen adsorption on the anatase TiO_2 (100) surface," *Journal of Molecular Structure: THEOCHEM*, vol. 868, no. 1-3, pp. 101–108, 2008.

[76] X. Yin, H. Han, I. Gunji, A. Endou, S. S. Cheettu Ammal, M. Kubo, and A. Miyamoto, "NH_3 adsorption on the Brönsted and Lewis acid sites of V_2O_5 (010): A periodic density functional study," *The Journal of Physical Chemistry B*, vol. 103, no. 22, pp. 4701–4706, 1999.

[77] I. Song, J. Lee, G. Lee, J. W. Han, and D. H. Kim, "Chemisorption of NH_3 on monomeric vanadium oxide supported on anatase TiO_2: A combined DRIFT and DFT study," *The Journal of Physical Chemistry C*, vol. 122, no. 29, pp. 16 674–16 682, 2018.

[78] D. Anderson and K. Burnham, "Model selection and multi-model inference," *Second. NY: Springer-Verlag*, vol. 63, no. 2020, p. 10, 2004.

[79] C. Chatfield, "Model uncertainty, data mining and statistical inference," *Journal of the Royal Statistical Society: Series A (Statistics in Society)*, vol. 158, no. 3, pp. 419–444, 1995.

[80] E. L. Lehmann, "Model specification: The views of Fisher and Neyman, and later developments," in *Selected Works of EL Lehmann*, Springer, 2012, pp. 955–963.

[81] G. E. Box, "Science and statistics," *Journal of the American Statistical Association*, vol. 71, no. 356, pp. 791–799, 1976.

[82] N. Oreskes, K. Shrader-Frechette, and K. Belitz, "Verification, validation, and confirmation of numerical models in the earth sciences," *Science*, vol. 263, no. 5147, pp. 641–646, 1994.

[83] W. Bechtel and A. Abrahamsen, "Explanation: A mechanist alternative," *Studies in History and Philosophy of Science Part C: Studies in History and Philosophy of Biological and Biomedical Sciences*, vol. 36, no. 2, pp. 421–441, 2005.

[84] R. N. Giere, "How models are used to represent reality," *Philosophy of science*, vol. 71, no. 5, pp. 742–752, 2004.

[85] J. W. Tukey, "We need both exploratory and confirmatory," *The American Statistician*, vol. 34, no. 1, pp. 23–25, 1980.

[86] H. Akaike, "A new look at the statistical model identification," *IEEE transactions on automatic control*, vol. 19, no. 6, pp. 716–723, 1974.

[87] C. Chatfield, "Avoiding statistical pitfalls," *Statistical Science*, pp. 240–252, 1991.

[88] G. E. Box and N. R. Draper, *Empirical model-building and response surfaces*. John Wiley & Sons, 1987.

[89] N. R. Draper and H. Smith, *Applied regression analysis*. John Wiley & Sons, 1998, vol. 326.

[90] Y. Gu, H.-L. Wei, and M. M. Balikhin, "Nonlinear predictive model selection and model averaging using information criteria," *Systems Science & Control Engineering*, vol. 6, no. 1, pp. 319–328, 2018.

[91] P. Atkins and J. De Paula, *Elements of physical chemistry*. Oxford University Press, USA, 2013.

[92] H. S. Fogler, *Essentials of Chemical Reaction Engineering*. Pearson Education, 2010.

[93] L. Lietti, I. Nova, S. Camurri, E. Tronconi, and P. Forzatti, "Dynamics of the SCR-DeNOx reaction by the transient-response method," *AIChE Journal*, vol. 43, no. 10, pp. 2559–2570, 1997.

[94] J. Wang and X. Guo, "Adsorption isotherm models: Classification, physical meaning, application and solving method," *Chemosphere*, vol. 258, p. 127 279, 2020.

[95] K. C. Ng, M. Burhan, M. W. Shahzad, and A. B. Ismail, "A universal isotherm model to capture adsorption uptake and energy distribution of porous heterogeneous surface," *Scientific Reports*, vol. 7, no. 1, pp. 1–11, 2017.

[96] K. Y. Foo and B. H. Hameed, "Insights into the modeling of adsorption isotherm systems," *Chemical engineering journal*, vol. 156, no. 1, pp. 2–10, 2010.

[97] B. Boulinguiez, P. Le Cloirec, and D. Wolbert, "Revisiting the determination of Langmuir parameters application to Tetrahydrothiophene adsorption onto activated carbon," *Langmuir*, vol. 24, no. 13, pp. 6420–6424, 2008.

[98] J. E. Cavanaugh and A. A. Neath, "The Akaike information criterion: Background, derivation, properties, application, interpretation, and refinements," *Wiley Interdisciplinary Reviews: Computational Statistics*, vol. 11, no. 3, e1460, 2019.

[99] J. Franklin, "The elements of statistical learning: Data mining, inference and prediction," *The Mathematical Intelligencer*, vol. 27, no. 2, pp. 83–85, 2005.

[100] M. Kuhn, K. Johnson, *et al.*, *Applied predictive modeling*. Springer, 2013, vol. 26.

[101] A. Airola, T. Pahikkala, W. Waegeman, B. De Baets, and T. Salakoski, "An experimental comparison of cross-validation techniques for estimating the area under the ROC curve," *Computational Statistics & Data Analysis*, vol. 55, no. 4, pp. 1828–1844, 2011.

[102] G. Shmueli, "To explain or to predict?" *Statistical science*, vol. 25, no. 3, pp. 289–310, 2010.